Supporting Information

TITLE: Antigen-Clustered Nanovaccine Achieves Long-Term Tumor Remission by Promoting B/CD 4 T Cell Crosstalk

AUTHOR NAMES

Chengyi Li[1,#], Ryan Clauson[1,#], Luke F. Bugada[2], Fang Ke[3], Bing He[4], Zhixin Yu[1], Hongwei Chen[1], Binyamin Jacobovitz[5], Hongxiang Hu[1], Polina Chuikov[3], Brett Dallas Hill[2], Syed M. Rizvi[2], Yudong Song[1], Kai Sun[6], Pasieka Axenov[3], Daniel Huynh[3], Xinyi Wang[1], Lana Garmire[4], Yu Leo Lei[7], Irina Grigorova[3], Fei Wen[2], Marilia Cascalho[3], Wei Gao[1,], Duxin Sun[1,*]*

AUTHOR ADDRESS

[1]Department of Pharmaceutical Sciences, College of Pharmacy, University of Michigan, Ann Arbor, Michigan 48109, United States

[2]Department of Chemical Engineering, College of Engineering, University of Michigan, Ann Arbor, Michigan 48109, United States

[3]Department of Microbiology and Immunology, Medical School, University of Michigan, Ann Arbor, Michigan 48109, United States

[4]Department of Computational Medicine & Bioinformatics, Medical School, University of Michigan, Ann Arbor, Michigan 48109, United States

[5]Microscopy Core, Medical School, University of Michigan, Ann Arbor, Michigan 48109, United States

[6]Department of Materials Science and Engineering, College of Engineering, University of Michigan, Ann Arbor, Michigan 48109, United States

[7]Departments of Head and Neck Surgery, Cancer Biology, and Translational Molecular Pathology, the University of Texas M.D. Anderson Cancer Center, Houston, Texas 77054, United States

[#]These contribute to this work equally.

*To whom correspondence should be addressed:

duxins@umich.edu (D Sun)

weiga@umich.edu (W Gao)

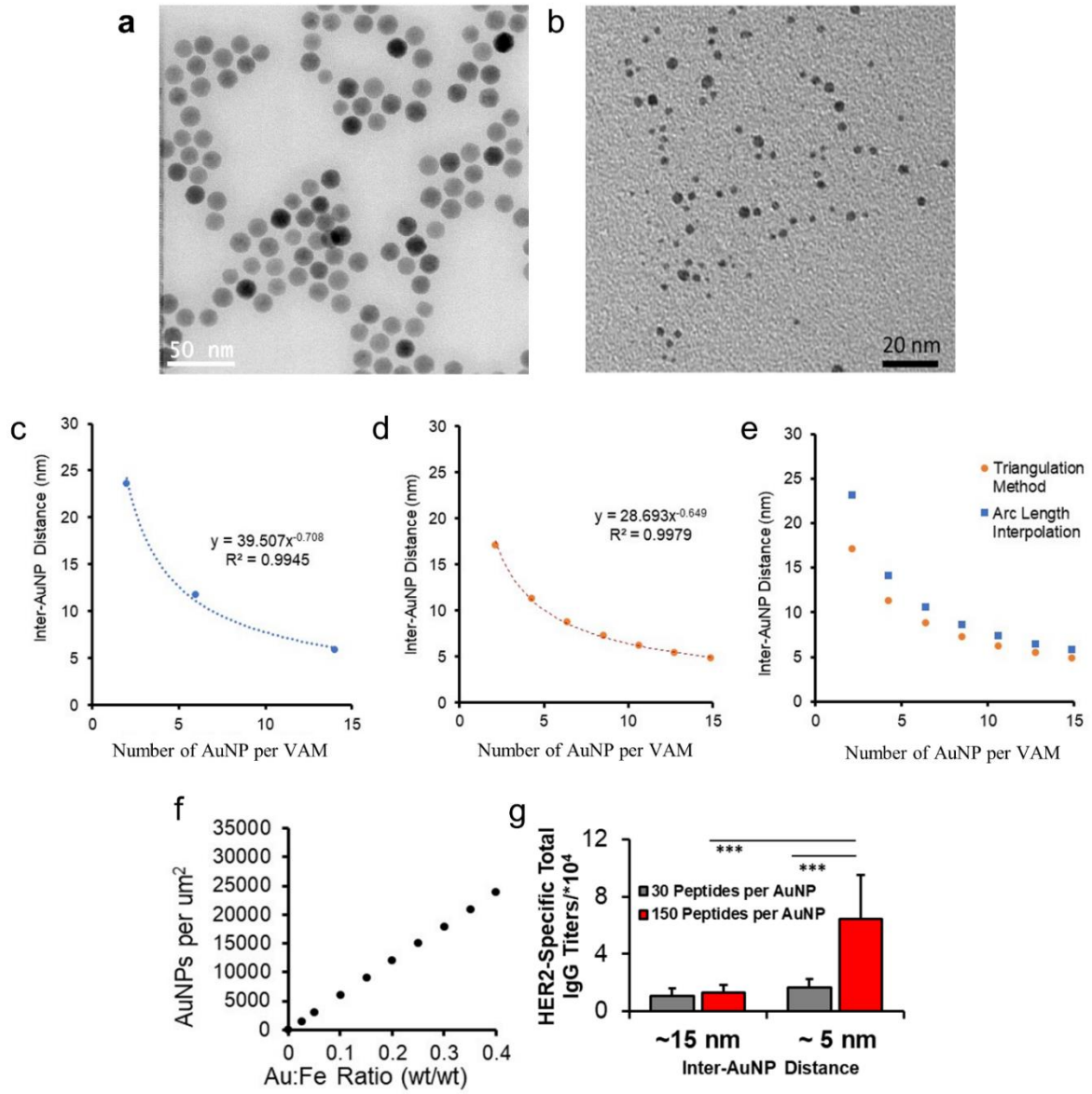

Figure S1. Characterizations of ACNVax. (**a**) Representative scanning transmission electron microscopy (STEM) bright-field (BF) image of the core component of ACN, poly(siloxane)- and poly (ethylene glycol)-containing di-block copolymer polymer-coated iron-oxide nanoparticle (IONP-Polymer); scale-bar: 50 nm. (**b**) Representative transmission electron microscopy (TEM) BF image of the surface component of gold nanoparticles (AuNP); scale-bar: 20 nm. (**c-e**) Modeling of inter-AuNP distance on antigen-clustered nanoparticle (ACN) surfaces. (**c**) Power function curve fit model based on the arc length between 2 (central angle: 180º), 6 (central angle: 90º) and 14 AuNPs (central angle: 45º) homogeneously distributed in 3D space around an IONP-Polymer core with 15 nm diameter. (**d**) Power function curve fit model based on the triangulation methodology described above. (**e**) Overlay comparison of both modeling strategies for inter-AuNP distance (nm). (**f**) AuNP density on ACN at different ratios between Au and Fe. (**g**) Quantification of antigen-specific IgG antibodies by ELISA after immunizations by ACNVax with different antigen cluster distances (5 or 15 nm) and different localized antigen densities (~30 and ~150 peptides/AuNPs). BALB/c mice were immunized at days 0 and 14, and antigen titers were detected at day 24; data represent the mean ± SD, n = 5. Statistical comparisons are based on one-way ANOVA, followed by post hoc Tukey's pairwise comparisons. The asterisks denote statistical significance at the level of *** $p < 0.001$. ANOVA, analysis of variance; SD, standard deviation.

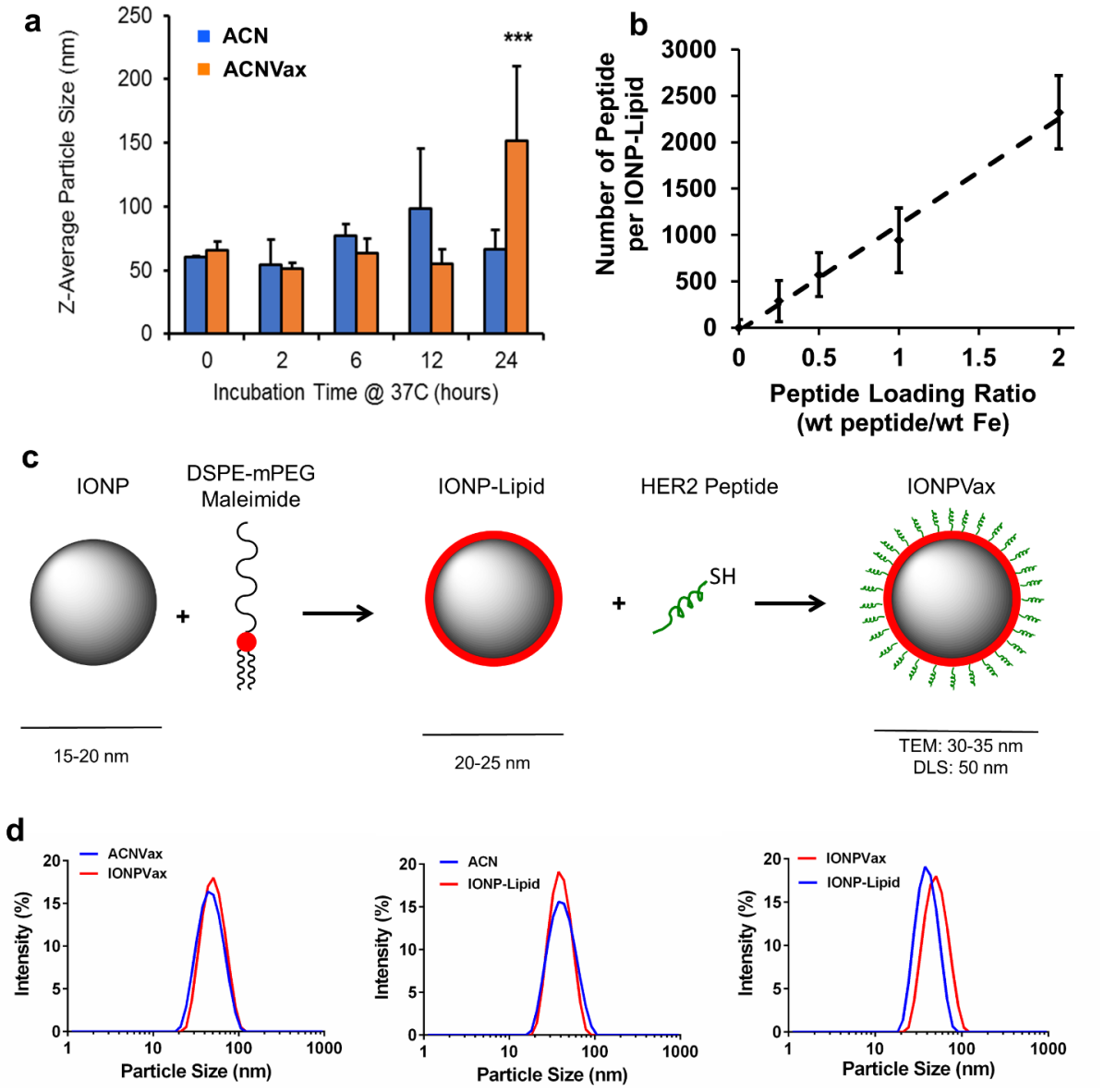

Figure S2. Characterizations of ACNVax and IONPVax. (**a**) Serum stability study of ACN and HER2 epitope coated ACNVax in 50% FBS/PBS at 37ºC as determined by Z-average particle size (nm) as determined by dynamic light scattering; data represent mean ± SD, n = 3. (**b**) Peptide loading at the surface of IONP-Lipid at different peptide to IONP ratio. (**c**) Schematic representation of step-wise formulation of peptide functionalized lipid-coated iron-oxide nanoparticles (IONP-Lipid) by the (1) coating of iron-oxide nanoparticles with maleimide activated DSPE-mPEG phospholipids followed by the (2) conjugation of terminal cysteine-modified HER2 peptide to IONP via non-reducing thiol-directed chemistry. (**d**) Representative volume-weighted particle size distributions: ACN, lipid-coated iron-oxide nanoparticles (IONP-Lipid), ACNVax and HER2 epitope coated IONP-Lipid (IONPVax). Statistical comparisons are based on one-way ANOVA, followed by post hoc Tukey's pairwise comparisons. The asterisks denote statistical significance at the level of *** $p < 0.001$. ANOVA, analysis of variance; SD, standard deviation.

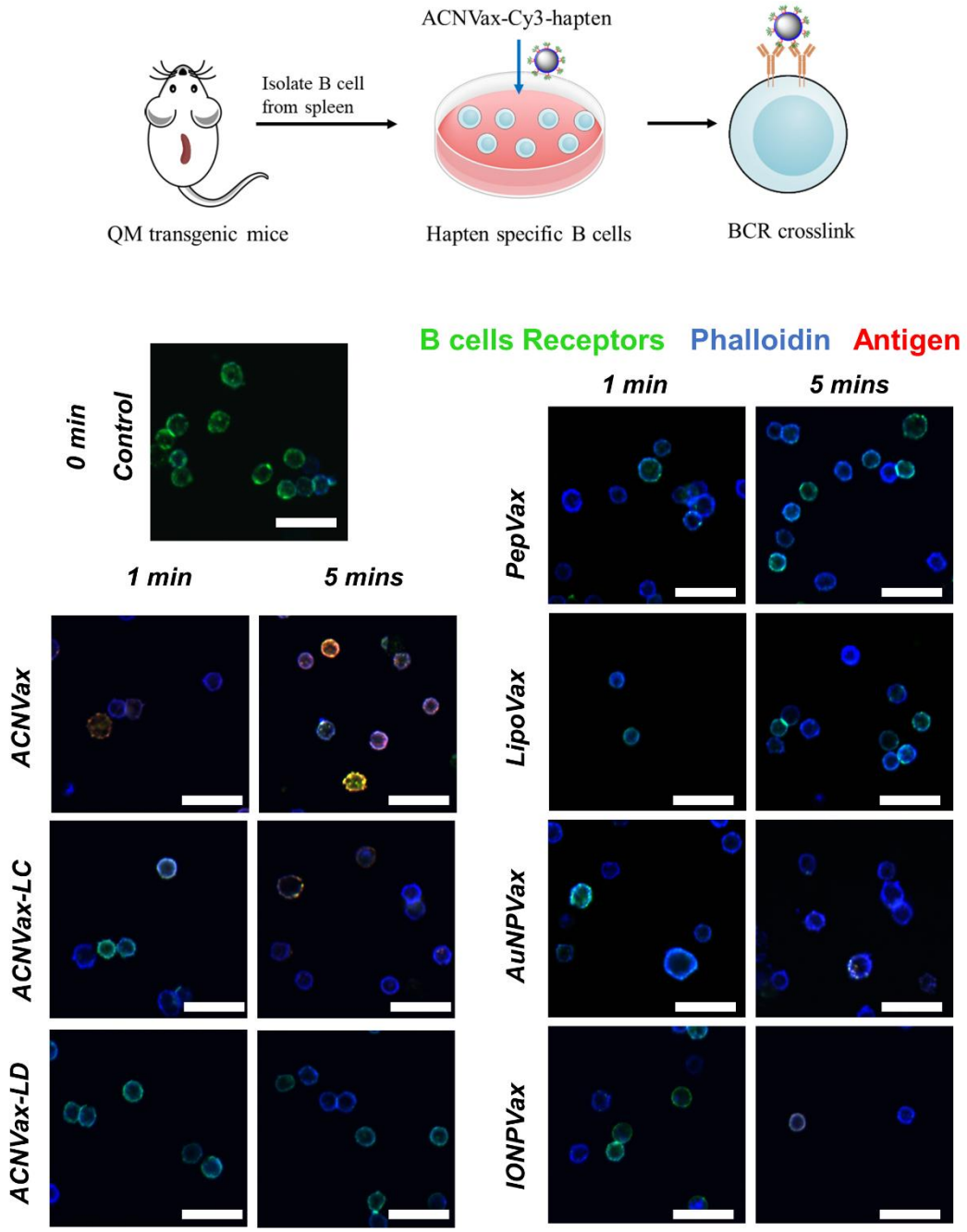

Figure S3. ACNVax crosslinked with B cell receptor. Confocal image of Cy3 and hapten labeled ACNVax (red, 20 nM antigens) binding/crosslinking (yellow) with B cell receptor (antibody staining, green) in hapten-specific B cells from QM mice splenocytes, in comparison with other control groups (20 nM antigens): soluble Cy3 and hapten labeled B/CD4 antigen (PepVax), Cy3 and hapten labeled IONPVax, Cy3 and hapten labeled AuNPVax, Cy3 and hapten labeled lipoVax, Cy3 and hapten labeled ACNVax with longer distance (~15 nm) between clusters (ACNVax-LC) and Cy3 and hapten labeled ACNVax with low density of antigen (2% of peptide loading, ACNVax-LD). Blue, phalloidin stain of actin filaments; green, B cell receptor staining using Alexa Fluor 488-AffiniPure Fab Fragment Goat Anti-Mouse IgM (μ Chain Specific) antibody; red: Cy3 and hapten-labeled CD4/B epitope. The scale bar is 10 μm.

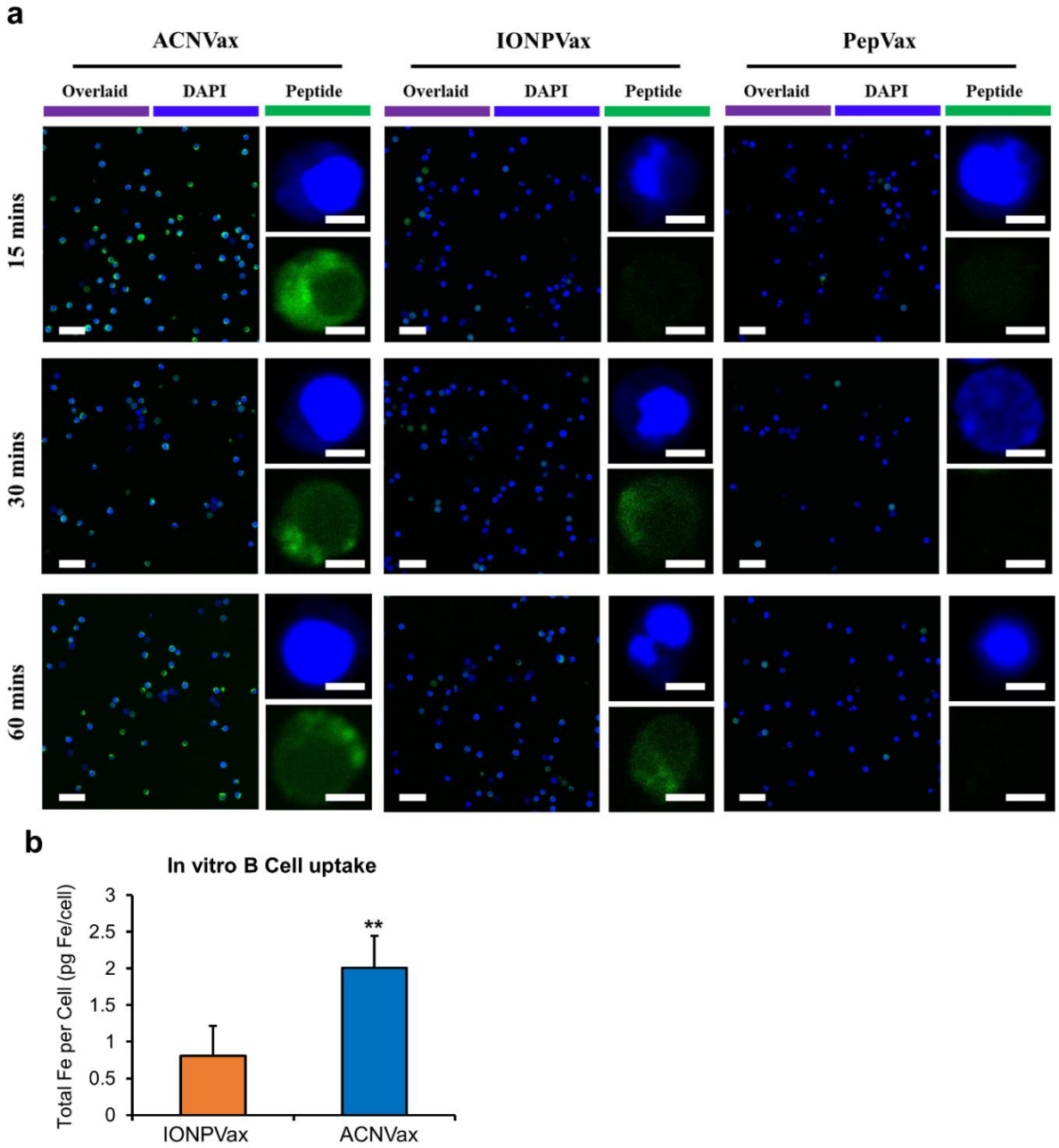

Figure S4. ACNVax enhanced antigen uptake by B cells. (**a**) Confocal image of ACNVax, IONPVax and PepVax uptake by B cells. Peptides are labeled by EDFITC. Nuclei are stained by DAPI. Incubation time points are 15 min, 30 mins and 60 mins. Scale bar for large images is 25 nm, for zoom in images are 2.5 nm. (**b**) Quantification of in-vitro cell uptake of nanoparticles in murine primary B-cells by ICP-MS quantification of total Fe standardized by cell count (pg Fe per cell). B-cells are identified as $B220^{+}$; data represent mean ± SD, n = 3. Data for quantification are shown as mean ± SD, n = 3. Statistical comparisons are based on one-way ANOVA, followed by post hoc Tukey's pairwise comparisons or by Student's unpaired T-test. The asterisks denote statistical significance at the level of * $p < 0.05$, ** $p < 0.01$. ANOVA, analysis of variance; SD, standard deviation.

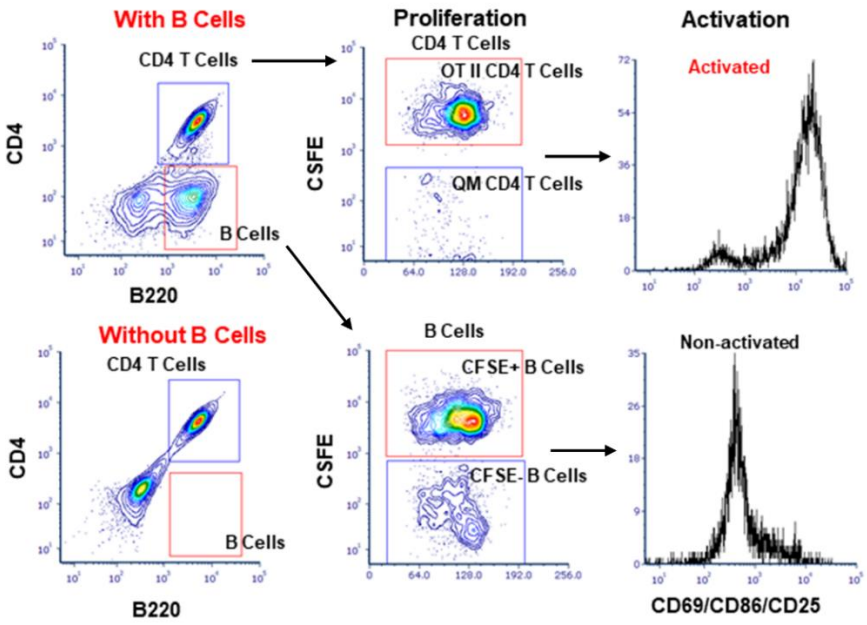

Figure S5. Gating strategy for flow cytometry analysis of B cell-antigen-presentation-mediated B/CD 4 T cell crosstalk by ACNVAX (Fig. 2, Fig. S5-S12). All CD4 T cells from OT-II mice and part of B cells from QM mice are labeled with CFSE tracker for proliferation observations. CD69 and CD86 are used as markers for CD4 T cell activation, CD69 and CD25 are used as markers for B cell activation.

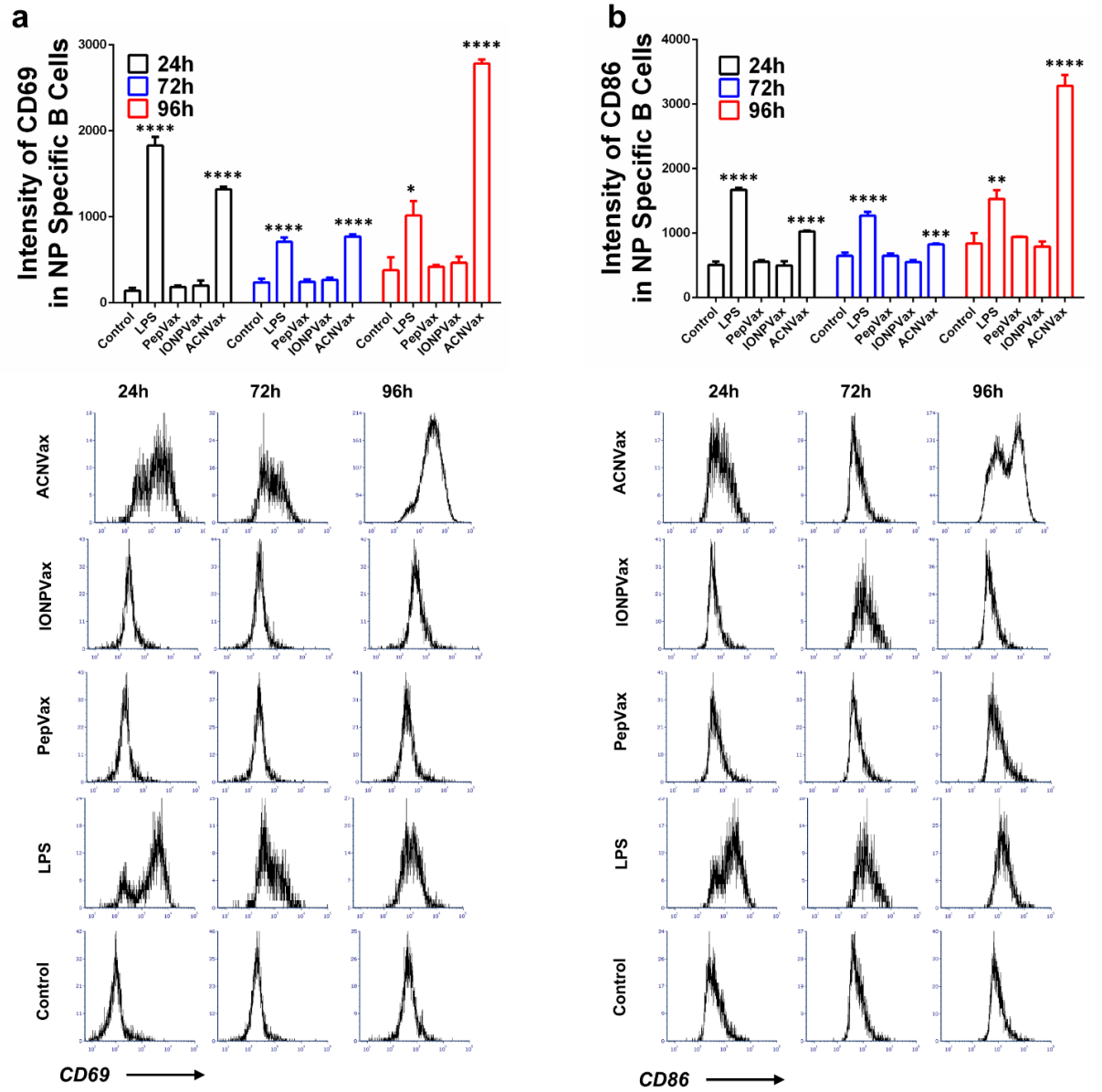

Figure S6. ACNVAX induced activation of antigen-specific B cells. Hapten-specific B cell activations were measured from 24h to 96h by increase of intensity of CD69 (**a**) and CD86 (**b**) markers. ACN with HER2-CD4/B antigen-Hapten and OT-II CD4 epitope was incubated with splenocytes from QM mice (part of B cells labeled with CFSE), and OT-II specific CD4 T cells (labeled with CFSE) from splenocytes of OT-II transgenic mice. IONP and free antigen peptides with the same antigens as ACNVax group were used as controls. Data for quantification are shown as mean ± SD, n = 3. Statistical comparisons are conducted among ACNVax and LPS with other groups. Statistical comparisons are based on one-way ANOVA, followed by post hoc Tukey's pairwise comparisons or by Student's unpaired T-test. The asterisks denote statistical significance at the level of * $p < 0.05$, ** $p < 0.01$, *** $p < 0.001$, **** $p < 0.0001$. ANOVA, analysis of variance; SD, standard deviation.

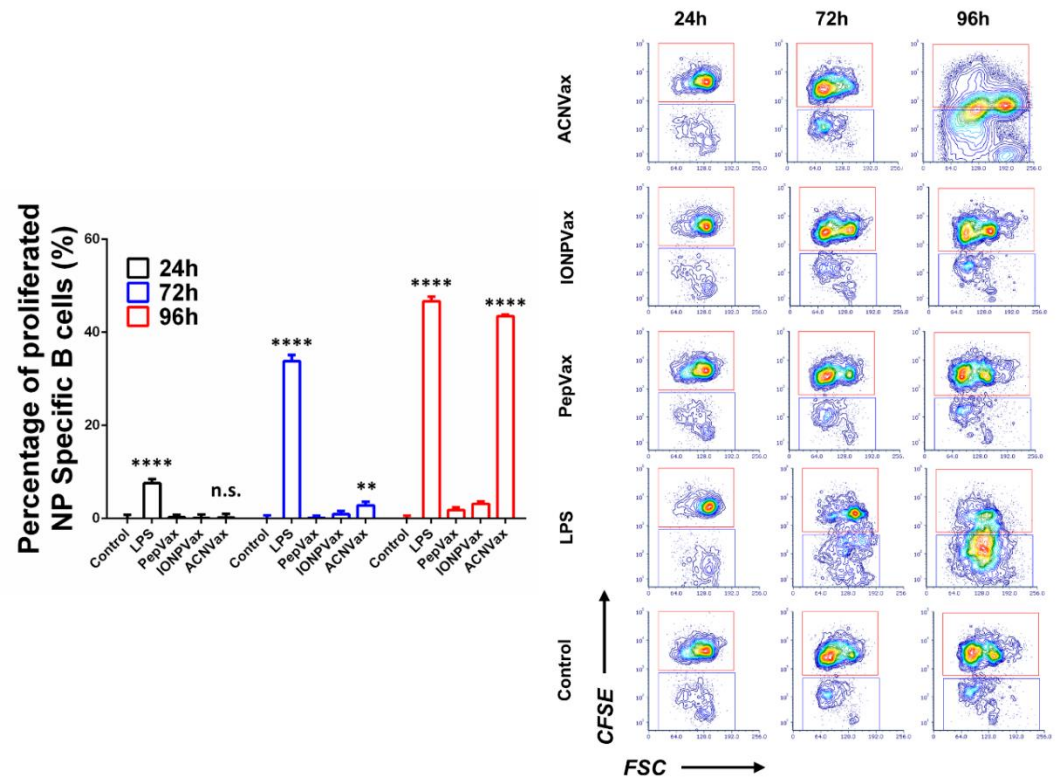

Figure S7. ACNVax induced proliferation of antigen-specific B cells. Representative flow cytometry analysis and quantification of Hapten-specific B cell proliferation by measuring the percentage of decreased $CFSE^{+}$ QM B cells compared to control. Data for quantification are shown as mean ± SD, n = 3. Statistical comparisons are conducted among ACNVax and LPS with other groups. Statistical comparisons are based on one-way ANOVA, followed by post hoc Tukey's pairwise comparisons or by Student's unpaired T-test. The asterisks denote statistical significance at the level of * $p < 0.05$, ** $p < 0.01$, *** $p < 0.001$, **** $p < 0.0001$. ANOVA, analysis of variance; SD, standard deviation; n.s., no statistical significance.

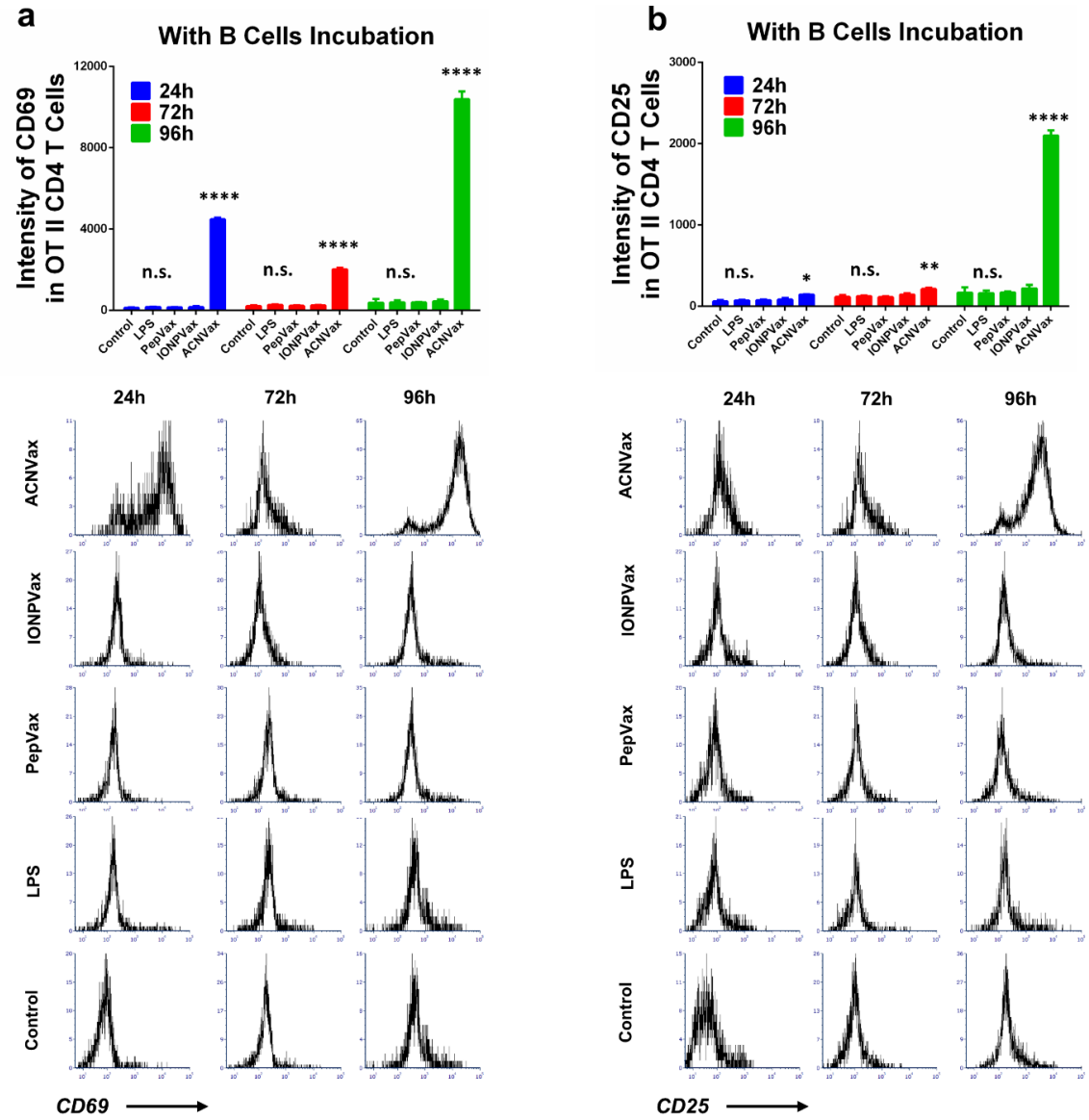

Figure S8. ACNVax induced activation of antigen-specific CD4 T cells. Activation of CD4 T cell from OT-II mice with B cells incubation were measured from 24h to 96h after incubation by increase of intensity of CD69 (**a**) and CD25 (**b**) markers. ACN with HER2-CD4/B antigen-hapten and OT-II CD4 epitope was incubated with splenocytes from QM mice (part B cells labeled with CFSE), and OT-II specific CD4 T cells (labeled with CFSE) from splenocytes of OT-II transgenic mice. IONP and free antigen peptides with the same antigens as ACNVax group were used as controls. Data for quantification are shown as mean ± SD, n = 3. Statistical comparisons are conducted among ACNVax and LPS with other groups. Statistical comparisons are based on one-way ANOVA, followed by post hoc Tukey's pairwise comparisons or by Student's unpaired T-test. The asterisks denote statistical significance at the level of * $p < 0.05$, ** $p < 0.01$, *** $p < 0.001$, **** $p < 0.0001$. ANOVA, analysis of variance; SD, standard deviation; n.s., no statistical significance.

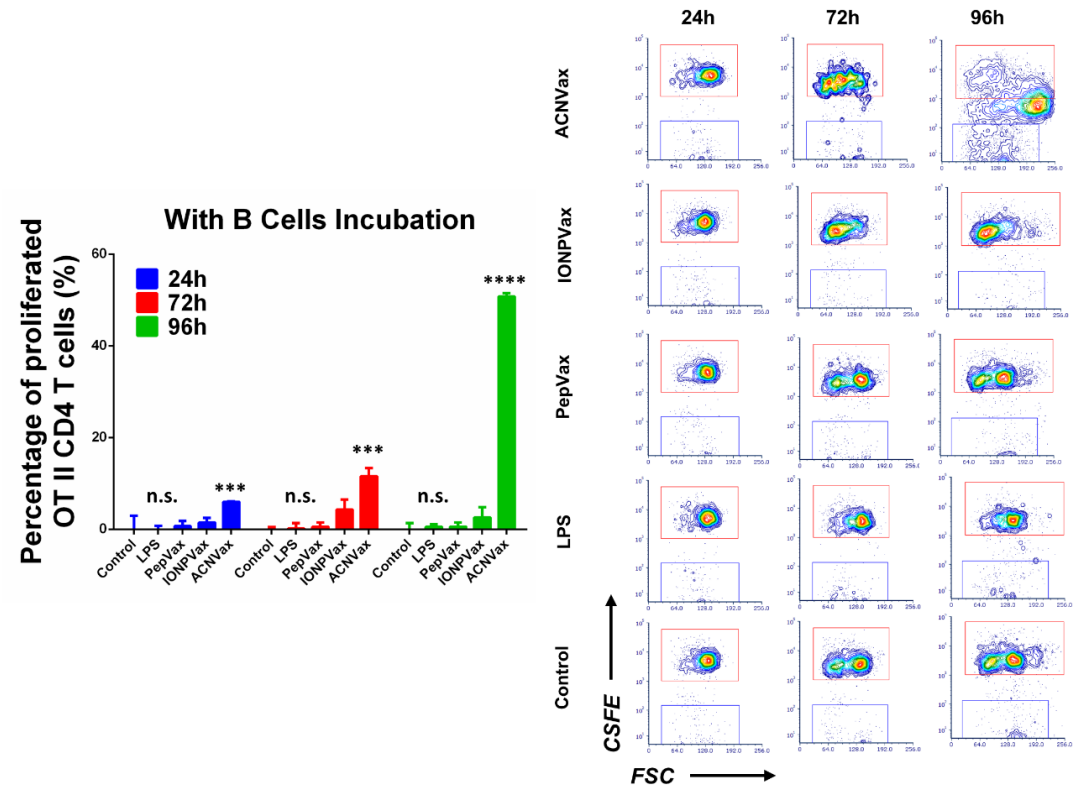

Figure S9. ACNVax induced proliferation of antigen-specific CD4 T cells. Representative flow cytometry analysis and quantification of OT-II specific CD4 T cell proliferation with B cells incubation by measuring the percentage of decreased CFSE+ OT-II specific CD4 T cells compared to control. Data for quantification are shown as mean ± SD, n = 3. Statistical comparisons are conducted among ACNVax and LPS with other groups. Statistical comparisons are based on one-way ANOVA, followed by post hoc Tukey's pairwise comparisons or by Student's unpaired T-test. The asterisks denote statistical significance at the level of * $p < 0.05$, ** $p < 0.01$, *** $p < 0.001$, **** $p < 0.0001$. ANOVA, analysis of variance; SD, standard deviation; n.s., no statistical significance.

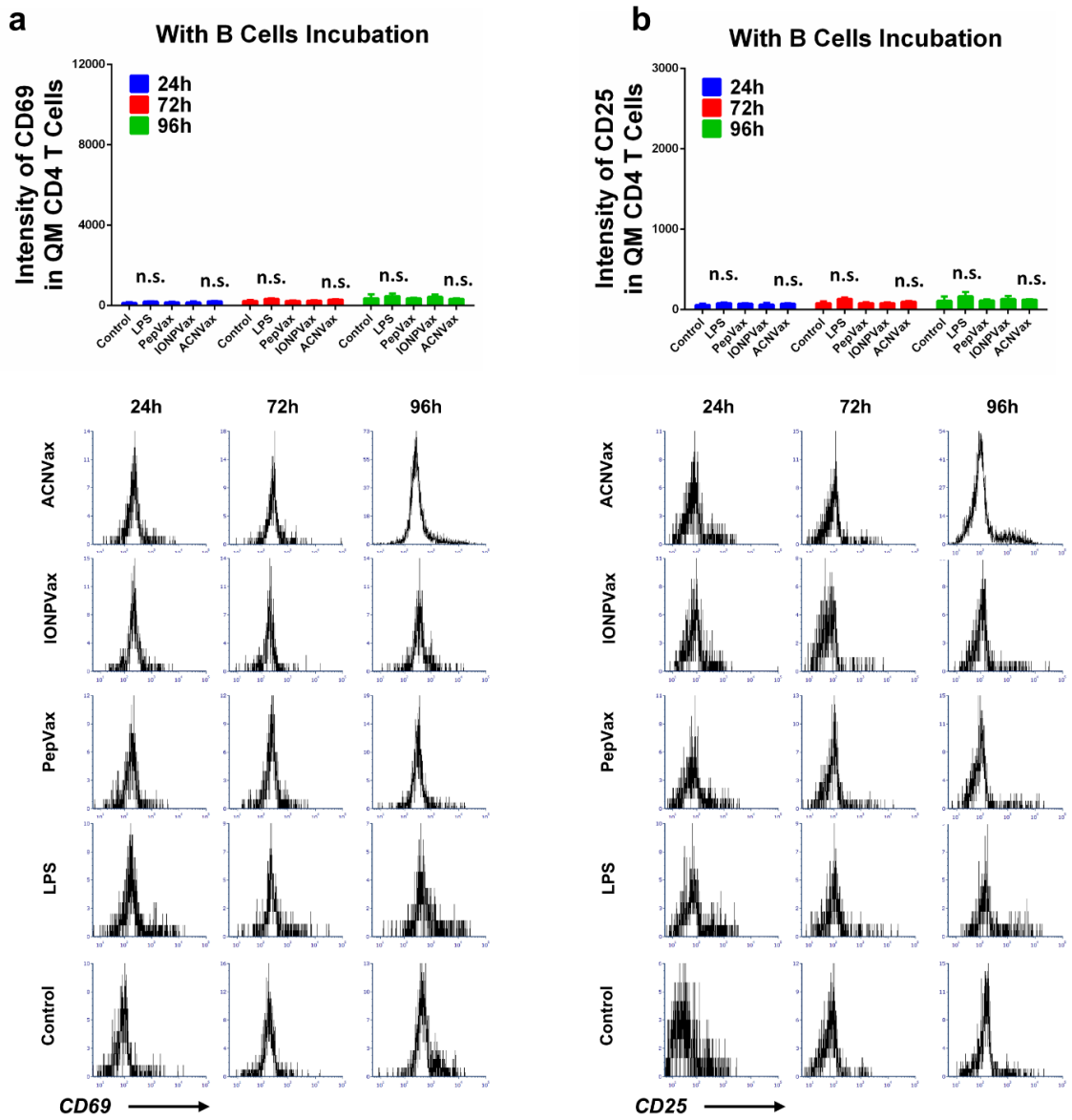

Figure S10. ACNVax did not induce activation of non-specific CD4 T cells. Activation of CD4 T cell from QM mice with B cells incubation were measured from 24h to 96h after incubation by increase of intensity of CD69 (**a**) and CD25 (**b**) markers. ACN with HER2-CD4/B antigen-hapten and OT-II CD4 epitope was incubated with splenocytes from QM mice (part B cells labeled with CFSE), and OT-II specific CD4 T cells (labeled with CFSE) from splenocytes of OT-II transgenic mice. IONP and free antigen peptides with the same antigens as ACNVax group were used as controls. Data for quantification are shown as mean ± SD, n = 3. Statistical comparisons are conducted among ACNVax and LPS with other groups. Statistical comparisons are based on one-way ANOVA, followed by post hoc Tukey's pairwise comparisons or by Student's unpaired T-test. ANOVA, analysis of variance; SD, standard deviation; n.s., no statistical significance.

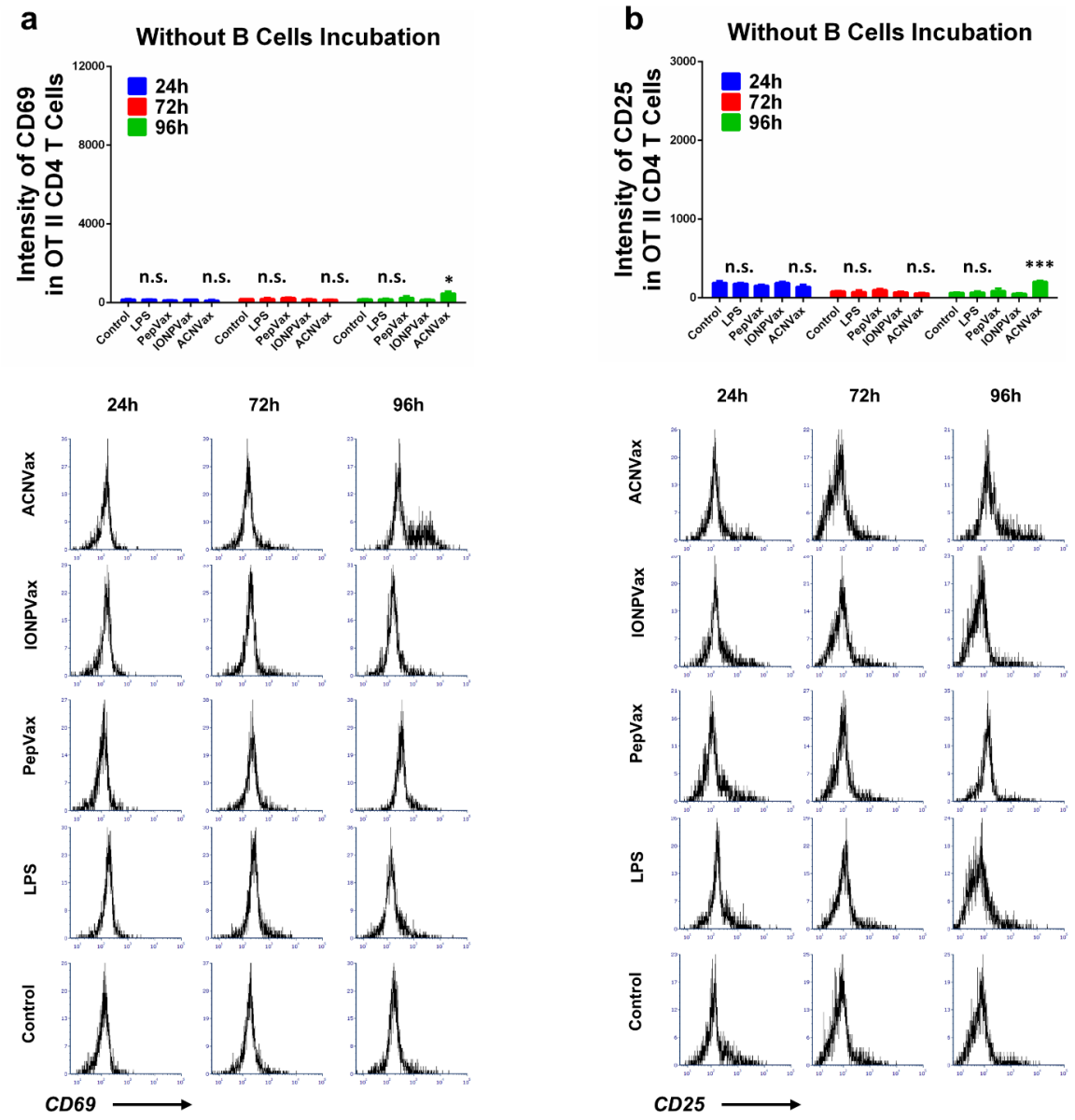

Figure S11. ACNVax did not induce activation of antigen-specific CD4 T cells after B cell depletion. Activation of CD4 T cell from OT-II mice without B cells incubation were measured from 24h to 96h after incubation by increase of intensity of CD69 (**a**) and CD25 (**b**) markers. (**c**) Proliferation of CD4 T cell from OT-II mice without B cells were measured from 24h to 96h by CFSE marker. ACN with HER2-CD4/B antigen-Hapten and OT-II CD4 epitope was incubated with splenocytes from QM mice (B cell depleted through CD19 positive selection kit), and OT-II specific CD4 T cells (labeled with CFSE) from splenocytes of OT-II transgenic mice. IONP and free antigen peptides with the same antigens as ACNVax group were used as controls. Data for quantification are shown as mean ± SD, n = 3. Statistical comparisons are conducted among ACNVax and LPS with other groups. Statistical comparisons are based on one-way ANOVA, followed by post hoc Tukey's pairwise comparisons or by Student's unpaired T-test. The asterisks denote statistical significance at the level of * $p < 0.05$, ** $p < 0.01$, *** $p < 0.001$. ANOVA, analysis of variance; SD, standard deviation; n.s., no statistical significance.

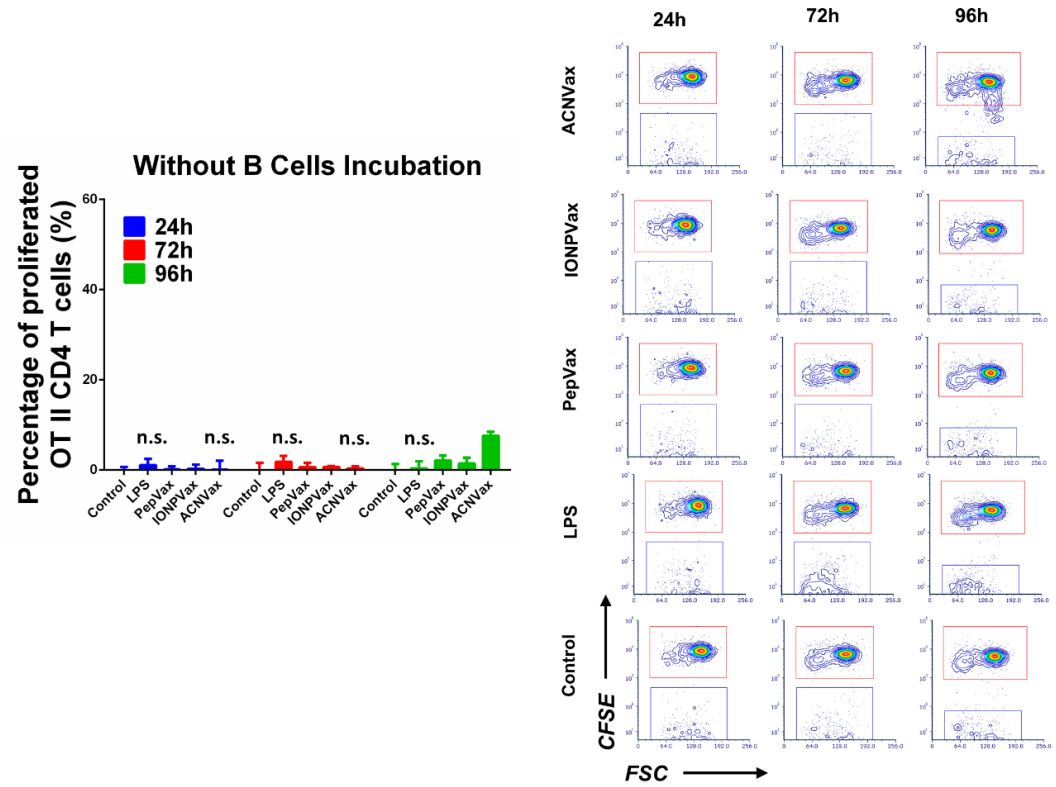

Figure S12. ACNVax did not induce proliferation of non-specific CD4 T cells after B cell depletion. Representative flow cytometry analysis and quantification of OT-II CD4 T cell proliferation without B cells incubation by measuring the percentage of decreased CFSE+ OT II CD4 T cells compared to control. Data for quantification are shown as mean ± SD, n = 3. Statistical comparisons are conducted among ACNVax and LPS with other groups. Statistical comparisons are based on one-way ANOVA, followed by post hoc Tukey's pairwise comparisons or by Student's unpaired T-test. The asterisks denote statistical significance at the level of * $p < 0.05$, ** $p < 0.01$. ANOVA, analysis of variance; SD, standard deviation; n.s., no statistical significance.

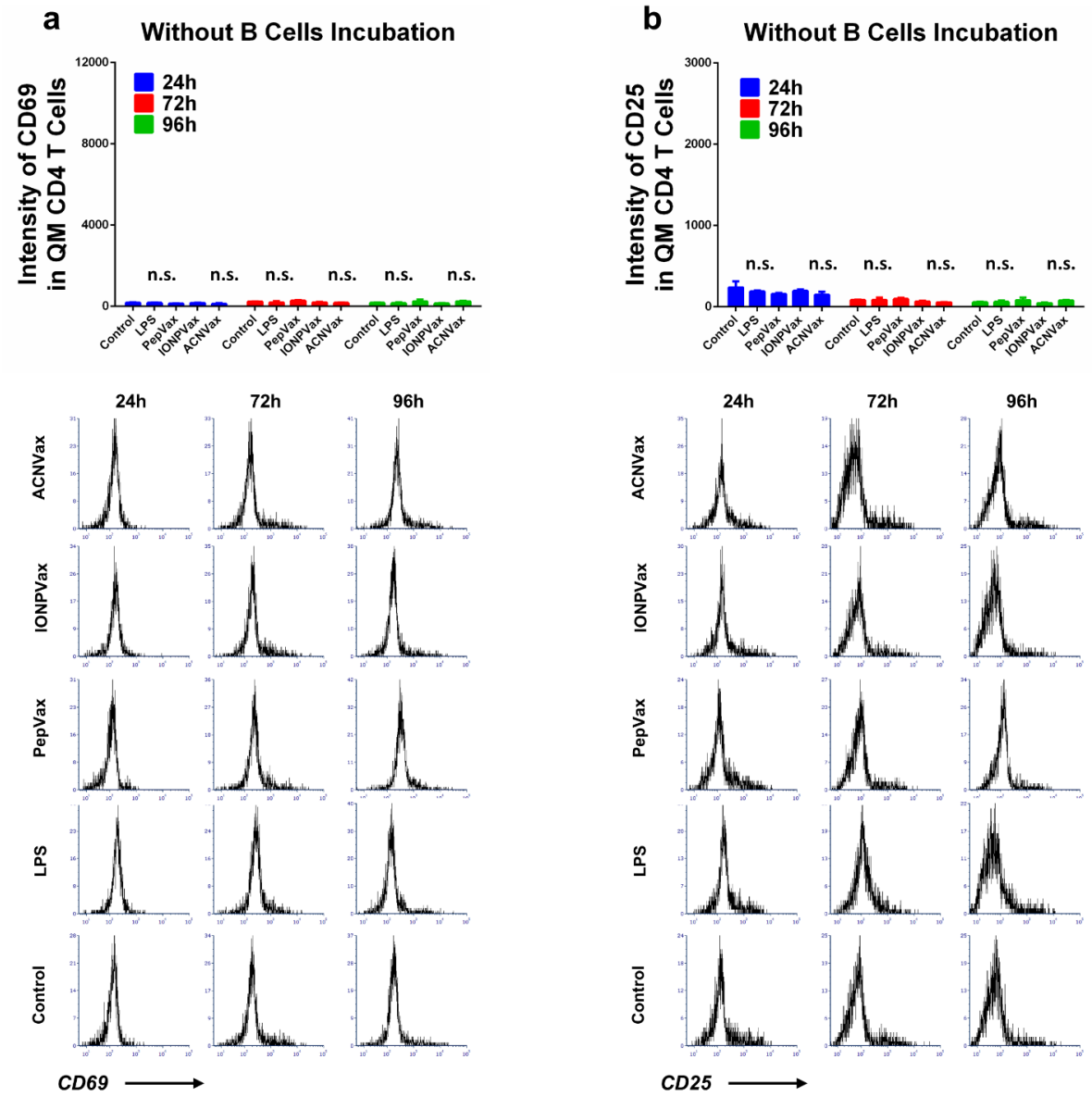

Figure S13. ACNVax did not induce activation of non-specific CD4 T cells after B cell depletion. Activation of CD4 T cell from QM mice without B cells incubation were measured from 24h to 96h after incubation by increase of intensity of CD69 (**a**) and CD25 (**b**) markers. ACN with HER2-CD4/B antigen-Hapten and OT-II CD4 epitope was incubated with splenocytes from QM mice (B cell depleted through CD19 positive selection kit), and OT-II specific CD4 T cells (labeled with CFSE) from splenocytes of OT-II transgenic mice. IONP and free antigen peptides with the same antigens as ACNVax group were used as controls. Data for quantification are shown as mean ± SD, n = 3. Statistical comparisons are conducted among ACNVax and LPS with other groups. Statistical comparisons are based on one-way ANOVA, followed by post hoc Tukey's pairwise comparisons or by Student's unpaired T-test. ANOVA, analysis of variance; SD, standard deviation; n.s., no statistical significance.

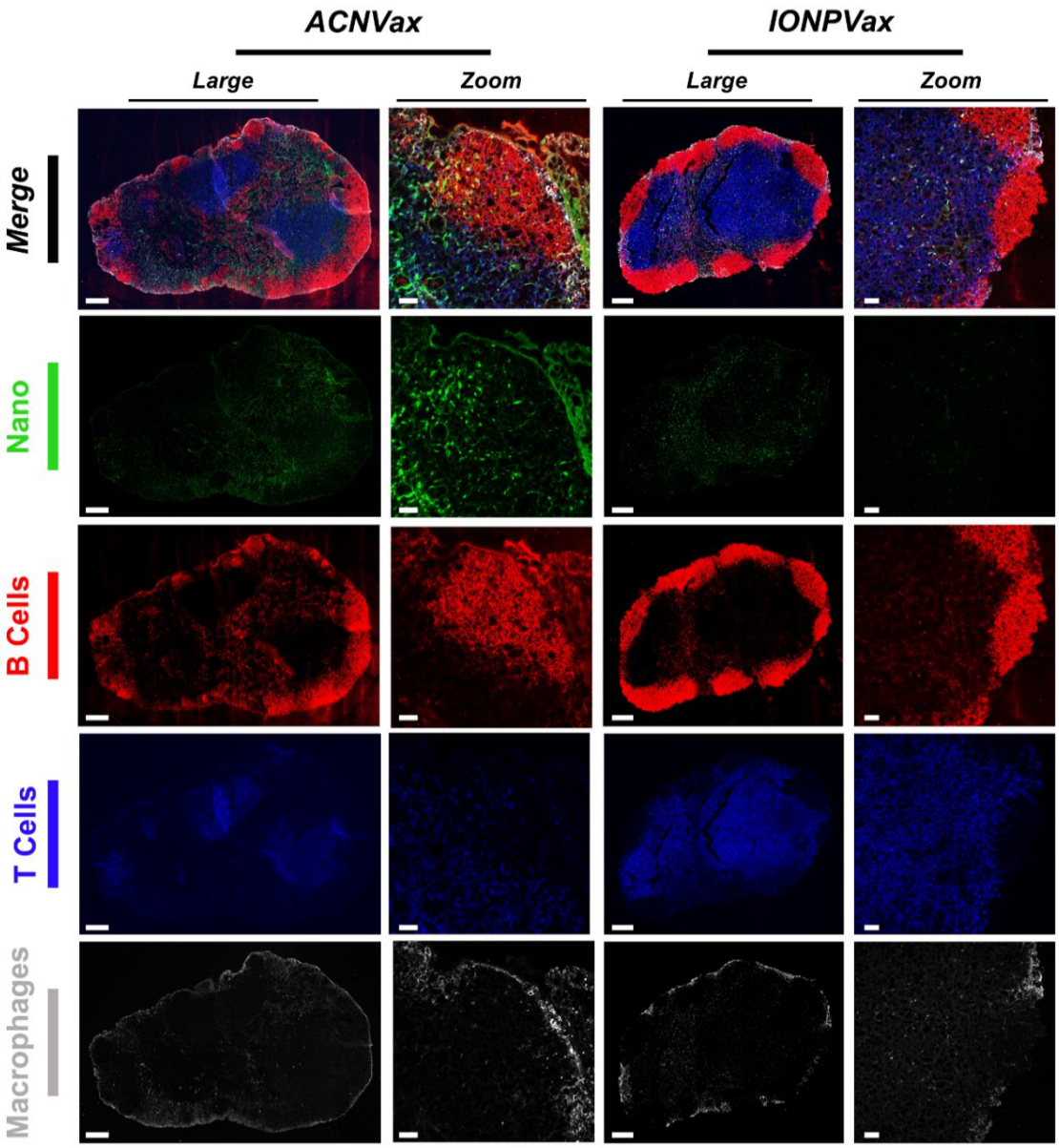

Figure S14. Confocal imaging of ACNVax and IONPVax lymph node distribution 12 hours after s.c injection in BALB/c mice. EDFITC labeled HER2 B/CD4 epitope are used as antigen conjugated to ACN or IONP. Brilliant Violet 421 B220, Alexa Fluor® 594 CD 3 and Alexa Fluor® 647 CD169 were used for lymph node staining. Scale bar is 200 µm for whole lymph node imaging and 50 µm for magnified images. Green channels: Antigens; Red channel: B Cells; Blue channels: T cells; Gray channels: Macrophages.

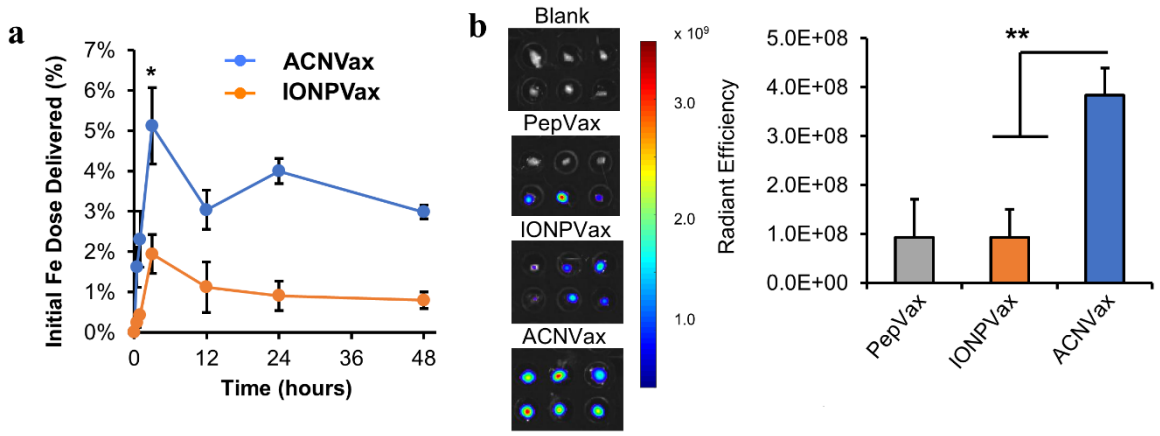

Figure S15. ACNVax enhanced delivery to lymph nodes. (**a**) Quantification of ACNVax and IONPVax delivery to lymph nodes (popliteal + inguinal) ipsilateral to the administration site at designated time intervals represented as the percentage of initial iron-oxide delivered using ICP-MS; data represent mean ± SE, n = 3. (**b**) Representative ex-vivo IVIS fluorescence images and semi-quantitative analysis (popliteal (top) + inguinal (bottom)) of peptide delivery to lymph nodes acquired 3 hours after administration of PepVax-Cy5.5, IONPVax-Cy5.5 and ACNVax-Cy5.5 (Ex/Em = 675/720 nm, exposure = 0.5 s). The color bar represents mean radiant efficiency (p/s/cm2/sr)/(μW/cm2); data represent mean ± SD, n = 3. Statistical comparisons are based on one-way ANOVA, followed by post hoc Tukey's pairwise comparisons or by Student's unpaired T-test. The asterisks denote statistical significance at the level of * $p < 0.05$, ** $p < 0.01$. ANOVA, analysis of variance; SD, standard deviation.

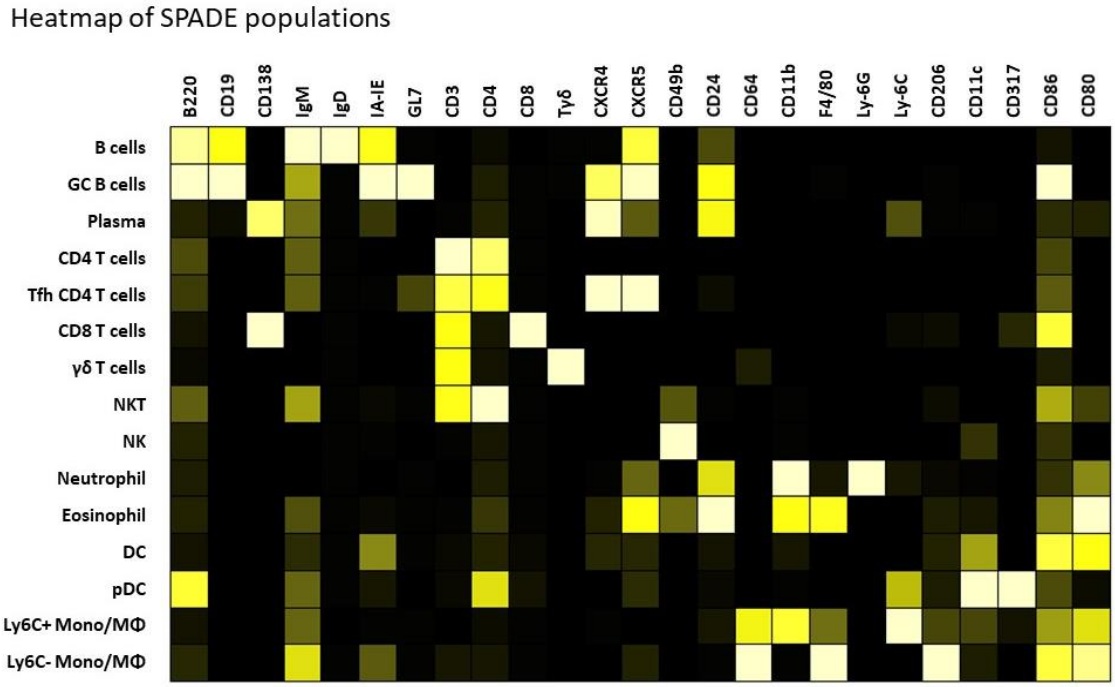

Figure S16. Heatmap showing marker expression of respective SPADE populations in lymph node and tumor. The heatmap values were calculated by dividing the median intensity of the marker in the given population by the maximum median intensity of the marker in all the populations.

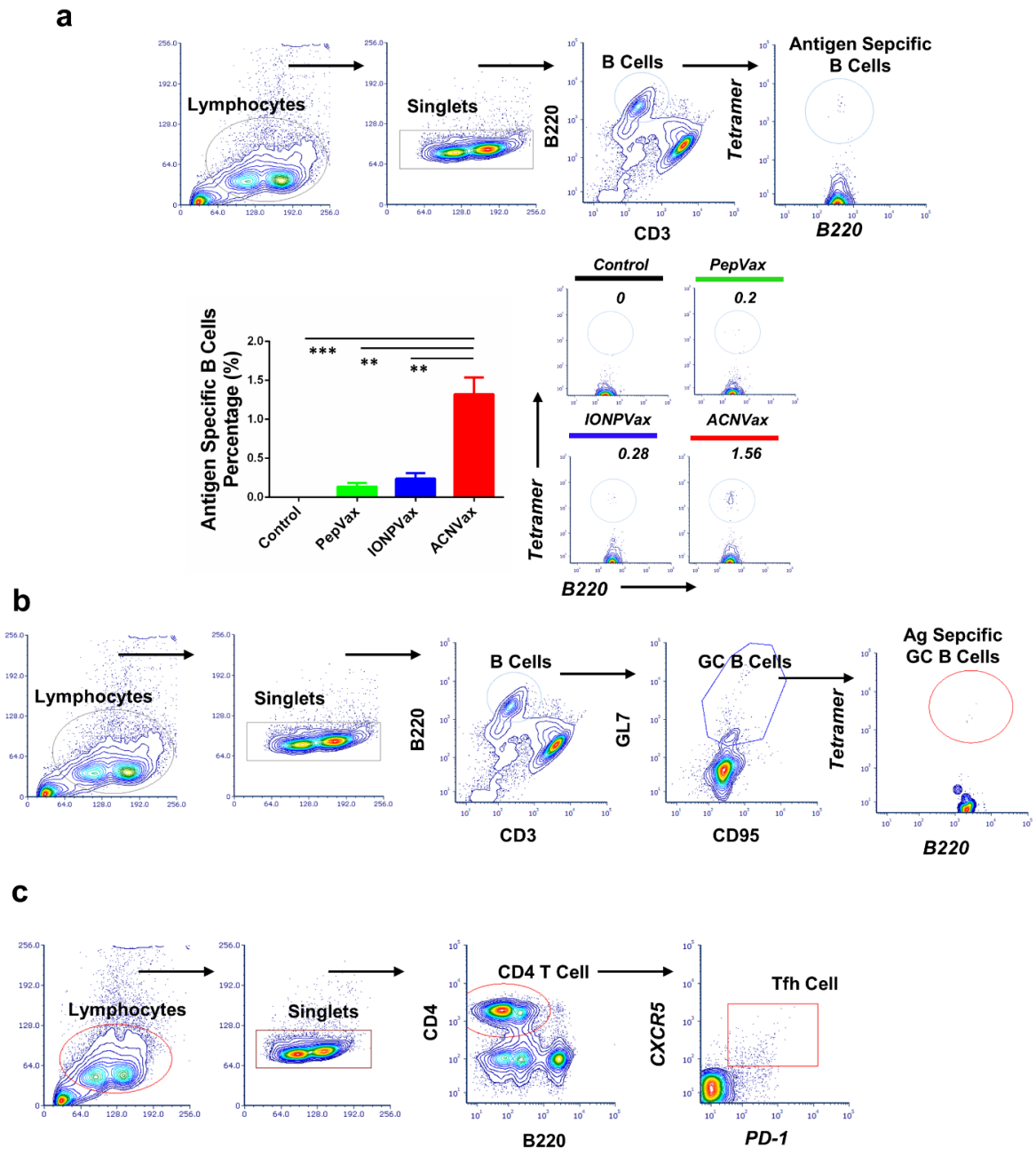

Figure S17. **ACNVax induced GC B cells, antigen-specific GC B cells, and Tfh cells in the lymph nodes.** Flow cytometry monitored GC B cells, antigen-specific GC B cells and Tfh cells in the lymph nodes after three vaccinations in BALB/c mice using control (PBS), PepVax, ACNVax or IONPVax (14.6 nmol antigen and 13.9 nmol 2'3'-cGAMP as adjuvant) at days 0, 7, and 14, and analyzed at day 24. (**a**) Gating strategy and representative flow cytometry analysis and quantification of antigen specific B cells. $CD3^{-}B220^{+}tetramer^{+}$ were identified as antigen specific B cells. (**b**) Gating strategy of Germinal center B cells and Germinal center derived HER2-specific B-cells in lymph nodes using B-cell receptor tetramer staining. $CD3^{-}$ $B220^{+}$ $CD95^{+}$ $GL\text{-}7^{+}$ populations were identified as GC B cells. (**c**) Gating strategy of Tfh cells. $B220^{-}CD4^{+}CXCR5^{+}PD\text{-}1^{+}$ populations were identified as Tfh cells. Data for quantification are shown as mean ± SD, n = 3. Statistical comparisons are based on one-way ANOVA, followed by post hoc Tukey's pairwise comparisons or by Student's unpaired T-test. The asterisks denote statistical significance at the level of * $p < 0.05$, ** $p < 0.01$, *** $p < 0.001$. ANOVA, analysis of variance; SD, standard deviation.

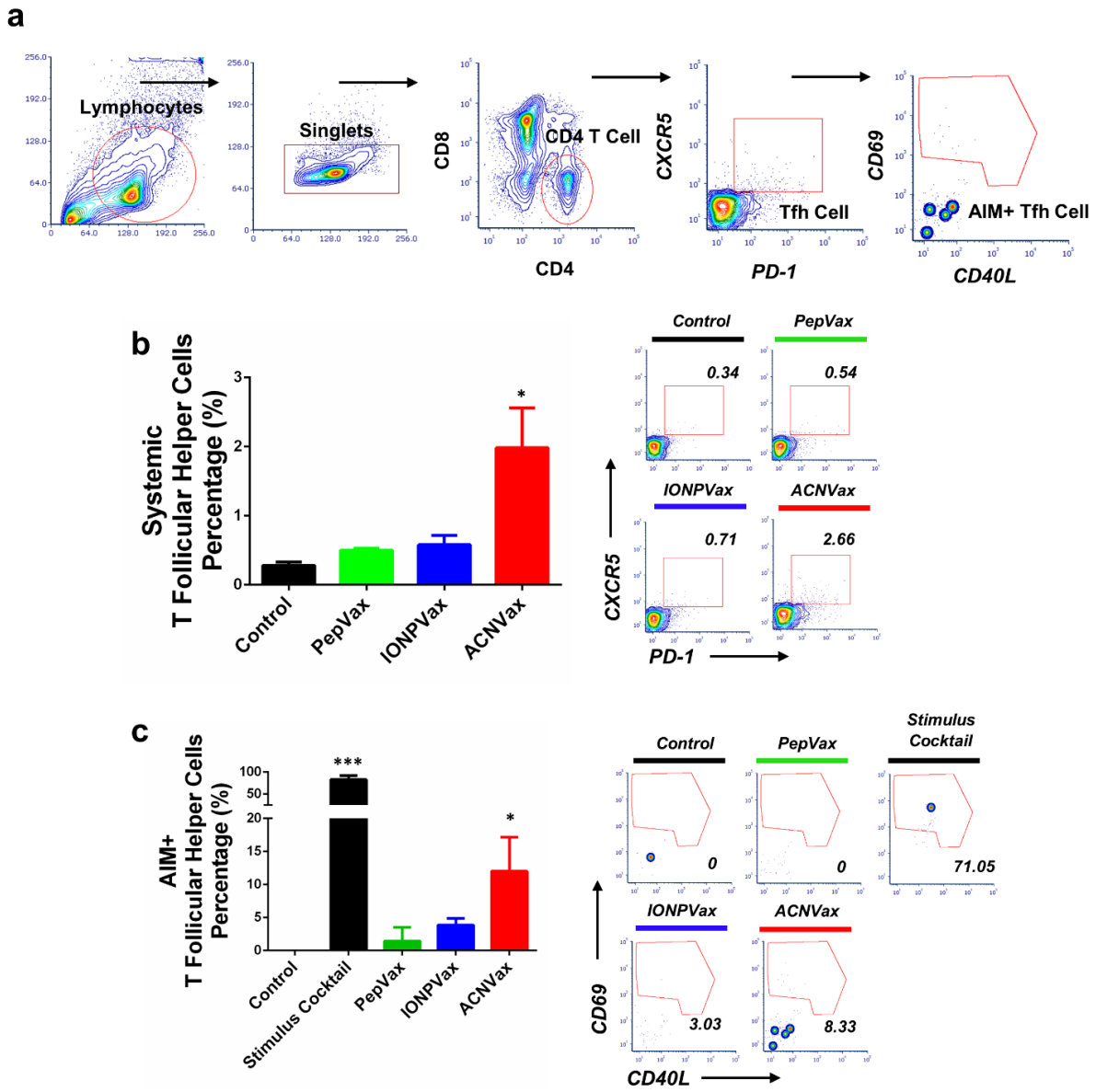

Figure S18. **ACNVax induced Tfh and AIM+ Tfh in the spleen.** Flow cytometry monitored Tfh and AIM+ Tfh cells in the spleen after three vaccinations in BALB/c mice using control (PBS), PepVax, ACNVax or IONPVax (14.6 nmol antigen and 13.9 nmol 2'3'-cGAMP as adjuvant) at days 0, 7, and 14, and analyzed at day 24. Gating strategy (**a**) and representative flow cytometry analysis and quantification of Tfh (**b**) and AIM+ Tfh (**c**) cells. $B220^{-}$ $CD4^{+}CXCR5^{+}PD\text{-}1^{+}$ populations were identified as Tfh cells. $CD69^{+}CD40L^{+/-}$ populations from Tfh cells were identified as AIM^{+} Tfh cells. Data for quantification are shown as mean ± SD, n = 3. Statistical comparisons are conducted among ACNVax with other groups. Statistical comparisons are based on one-way ANOVA, followed by post hoc Tukey's pairwise comparisons or by Student's unpaired T-test. The asterisks denote statistical significance at the level of * $p < 0.05$, ** $p < 0.01$, *** $p < 0.001$. ANOVA, analysis of variance; SD, standard deviation.

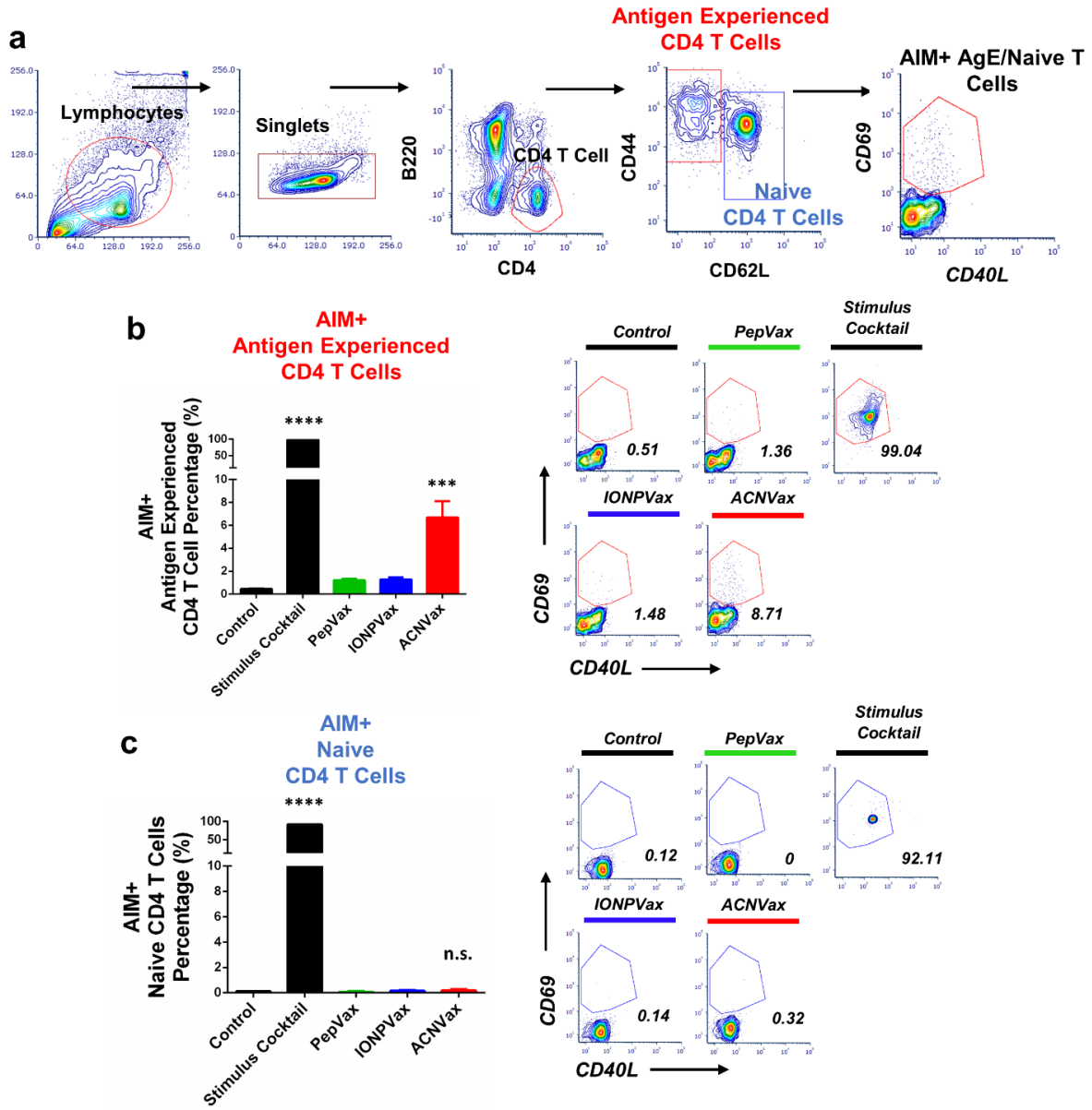

Figure S19. **ACNVax induced AIM+ CD4 T cells.** Flow cytometry monitored AIM+ antigen experienced CD4 T and AIM+ naïve CD4 T cells in the spleen after three vaccinations in BALB/c mice using control (PBS), PepVax, ACNVax or IONPVax (14.6 nmol antigen and 13.9 nmol 2'3'-cGAMP as adjuvant) at days 0, 7, and 14, and analyzed at day 24. Gating strategy (**a**) and representative flow cytometry analysis and quantification of AIM+ antigen experienced CD4 T (**b**) and AIM+ naïve CD4 T cells (**c**). $B220^{-}CD4^{+}CD62L^{+}CD69^{+}CD40L^{+/-}$ populations were identified as AIM^{+} antigen experienced CD4 T cells. $B220^{-}CD4^{+}CD62L^{-}CD69^{+}CD40L^{+/-}$ populations were identified as AIM+ naïve CD4 T cells. Data for quantification are shown as mean ± SD, n = 3. Statistical comparisons are conducted among ACNVax with other groups. Statistical comparisons are based on one-way ANOVA, followed by post hoc Tukey's pairwise comparisons or by Student's unpaired T-test. The asterisks denote statistical significance at the level of * $p < 0.05$, ** $p < 0.01$, *** $p < 0.001$, **** $p < 0.0001$.

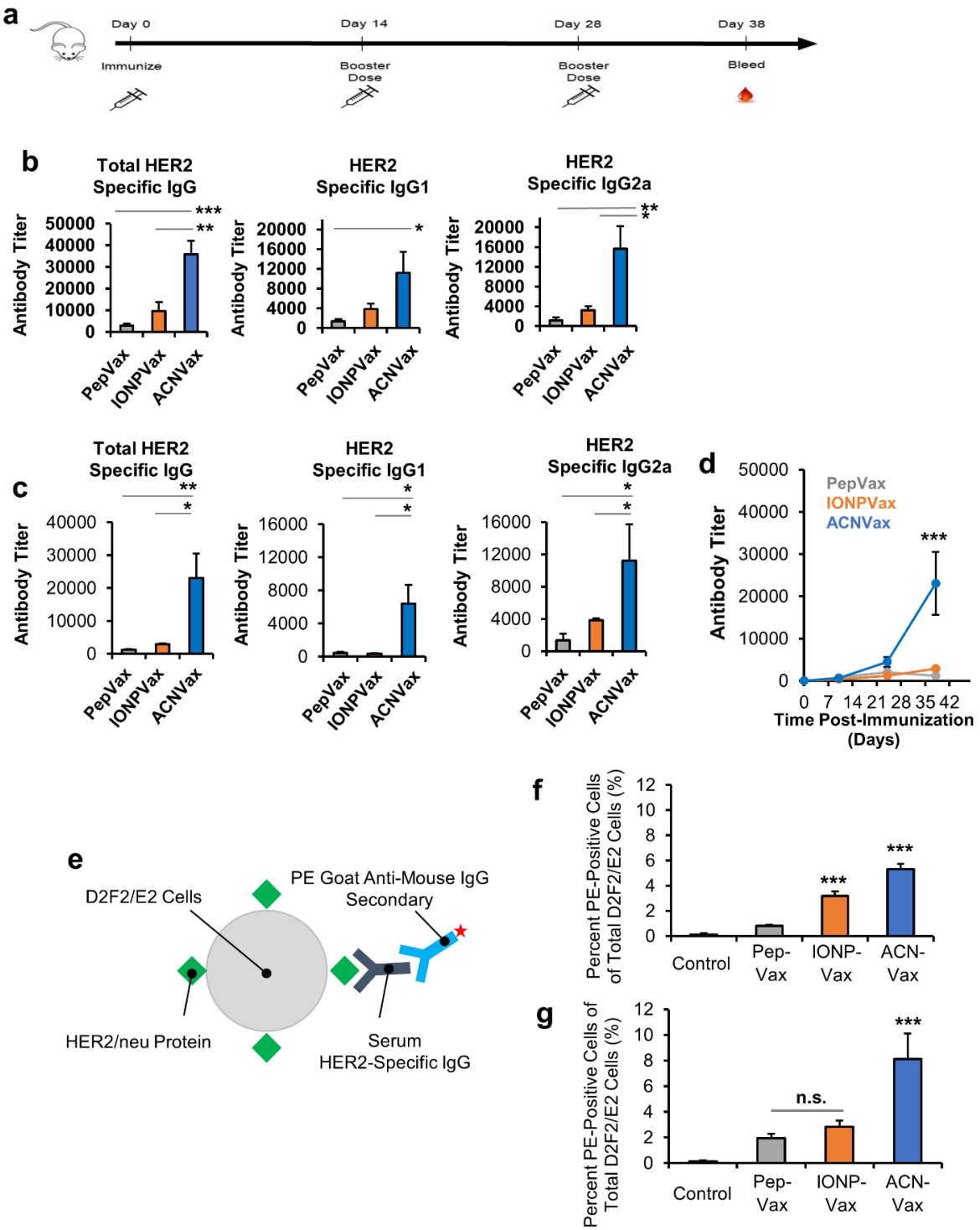

Figure S20. ACNVax induced production of HER2-specific antibody. (**a**) Animal study immunization and analytical sampling timeline. (**b-d**) Quantification of antigen-specific IgG antibodies by indirect ELISA represented as antibody titer from serum collected 10 days after every immunization (day 10, day 24 and day 38) with either (**b**) 50 µg HER2 peptide (14.6 nmol) dose + 10 µg cGAMP or (**c,d**) 5 µg HER2 peptide dose + 10 µg cGAMP; data represent mean ± SD, n = 5. (**e-g**) Antibody specificity binding to HER-2 positive (D2F2/E2) cell. (**e**) Schematic representation of the flow cytometry detection of anti-HER2 antibody binding specificity to D2F2/E2 cells using PE-labeled IgG secondary antibody detection. Anti-HER2 antibody binding specificity to D2F2/E2 cells of serum obtained from mice immunized with (**f**) 5 µg HER2 peptide dose + 10 µg cGAMP or (**g**) 50 µg HER2 peptide dose + 10 µg cGAMP; data represent mean ± SD, n = 3. Statistical comparisons are based on one-way ANOVA,

followed by post hoc Tukey's pairwise comparisons. The asterisks denote statistical significance at the level of * $p < 0.05$, ** $p < 0.01$, *** $p < 0.001$. ANOVA, analysis of variance; SD, standard deviation; n.s., no statistical significance.

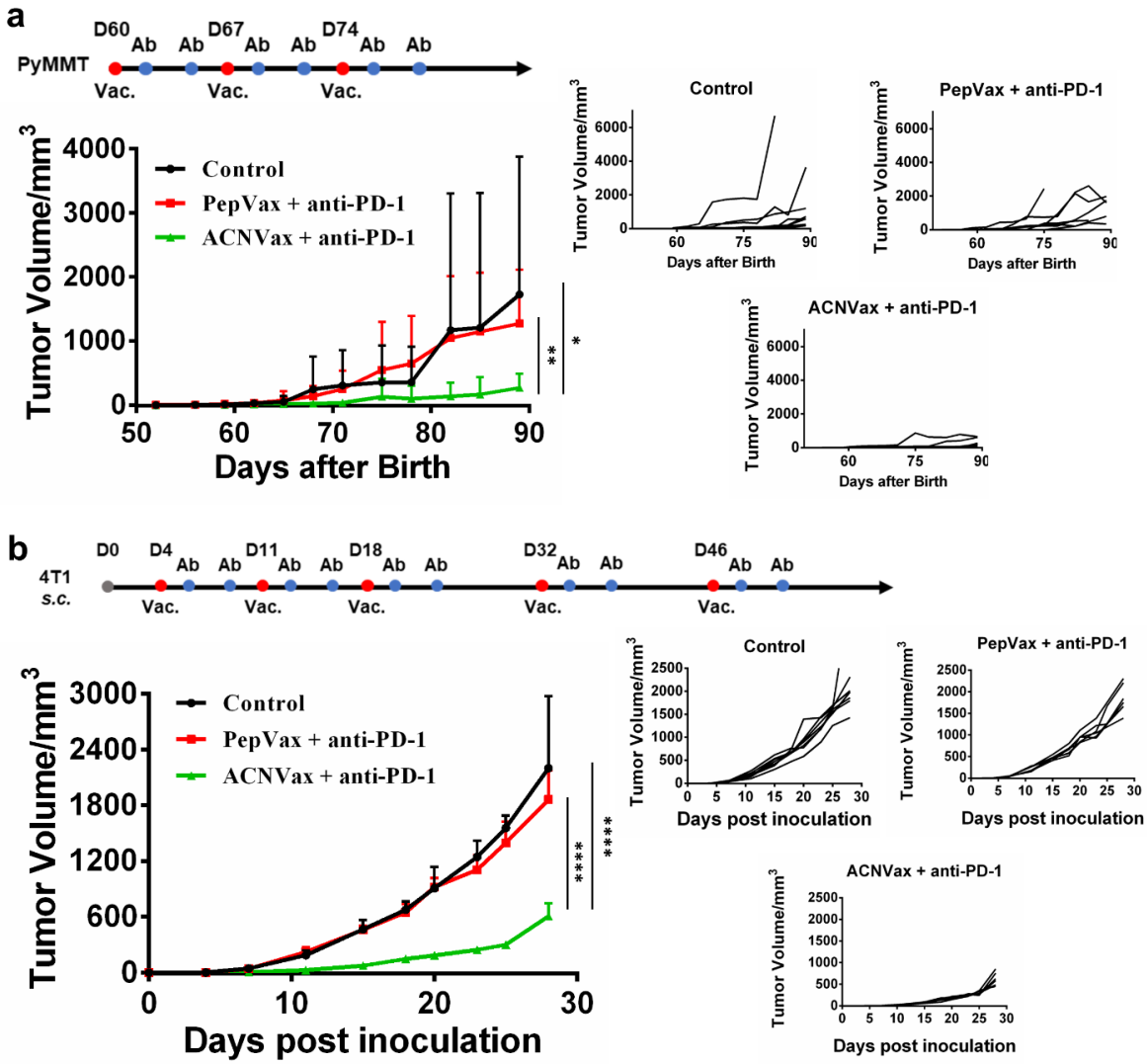

Figure S21. Antitumor efficacy of ACNVax on transgenic PyMT-MMTV breast cancer (a) and 4T1 xenograft breast cancer (b) models. For each vaccine, we used 14.6 nmol epitopes with 13.9 nmol 2′3′-cGAMP as the adjuvant. Data represent the mean ± SD, n = 8 for all PyMT-MMTV groups, n=7 for the control, PepVax + anti-PD-1 and ACNVax + anti-PD-1 groups from 4T1 subcutaneous breast cancer model. Mouse HER2 epitope were used as antigen in the test: CDDDPESFDGNPSSGVAPLKPEHLQ (Mouse HER2 CD4/B cell epitope). Statistical comparisons are based on one-way ANOVA, followed by post hoc Tukey's pairwise comparisons. The asterisks denote statistical significance at the level of * $p < 0.05$, ** $p < 0.01$, *** $p < 0.001$, **** $p < 0.0001$. ANOVA, analysis of variance; SD, standard deviation; n.s., no statistical significance.

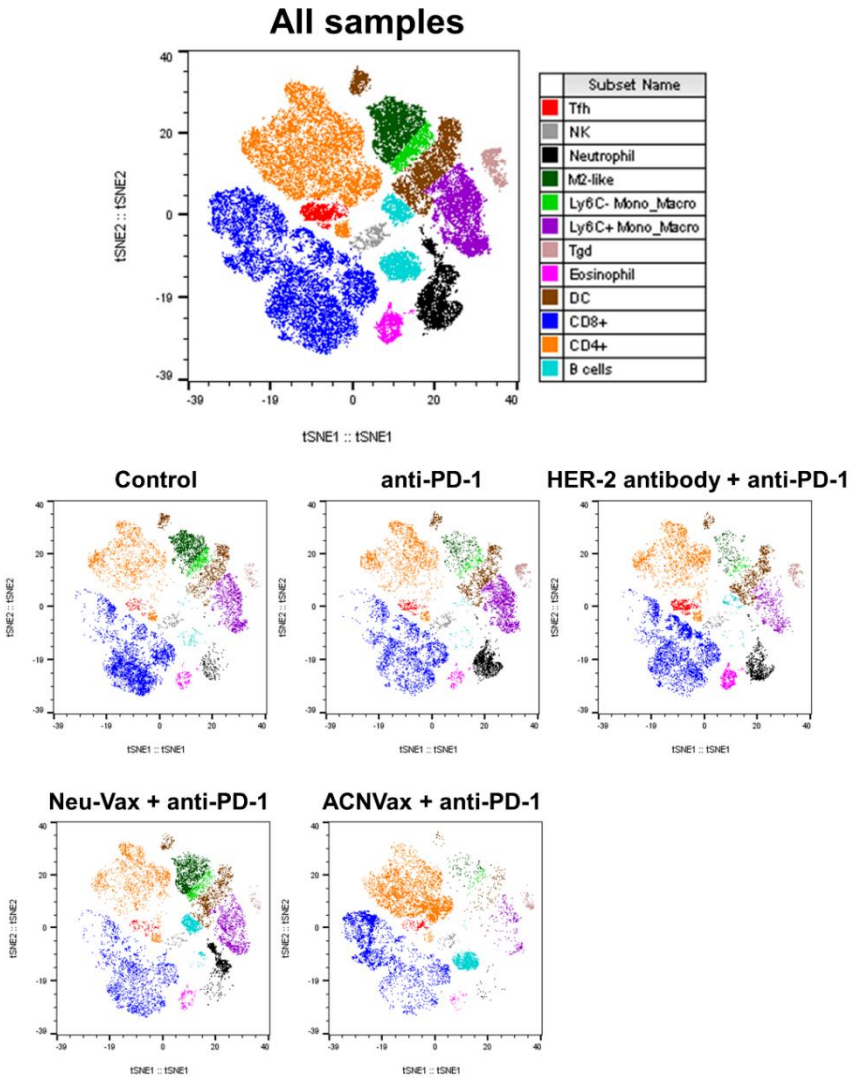

Figure S22. t-distributed stochastic neighbor embedding (TSNE) analysis of tumor infiltrating immune cells from CyTOF analysis results in Balb/c mice with HER2+ breast cancer by different treatment. Tumor samples were harvested and dissociated into single cell suspension 10 days after the second boost of vaccination. CyTOF antibody conjugation and data acquisition were done as previously described[1, 2]. CyTOF data analysis was performed as previously described[2]. All events were gated to remove noncellular events (negative for DNA intercalator), dead cells (negative for uptake of cisplatin) and doublets. viSNE analysis were performed using the Cytobank platform.

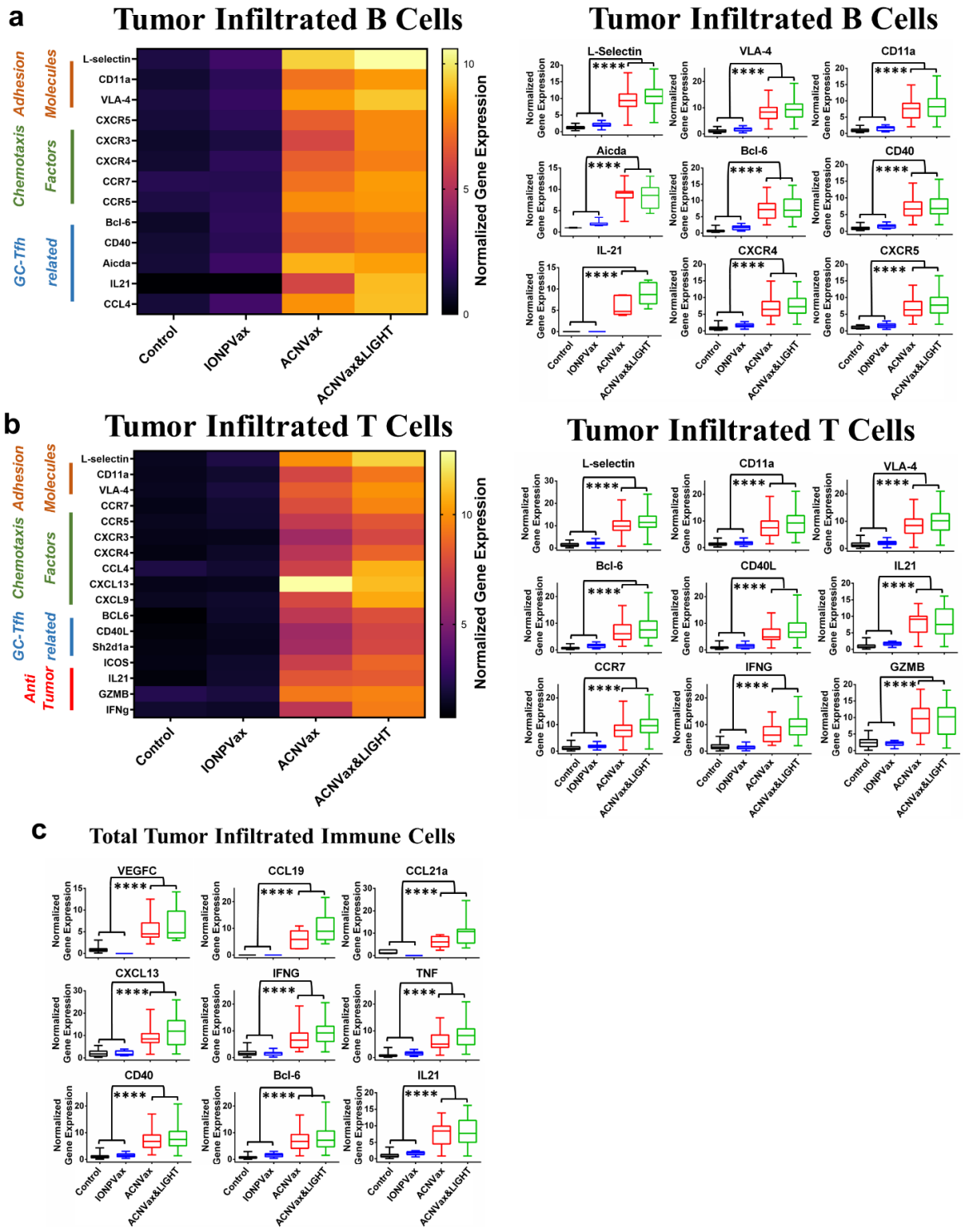

Figure S23. ACNVax induced various gene expression in tumor infiltrating B cells, T cells and total immune cells. Heatmap and boxplots of selected gene expression levels in tumor infiltrated B cells (**a**), T cells (**b**) and total immune cells (**c**) from single-cell RNA sequencing. Statistical comparisons are based on one-way ANOVA, followed by post hoc Tukey's pairwise comparisons. The asterisks denote statistical significance at the level of **** $p < 0.0001$. ANOVA, analysis of variance; SD, standard deviation.

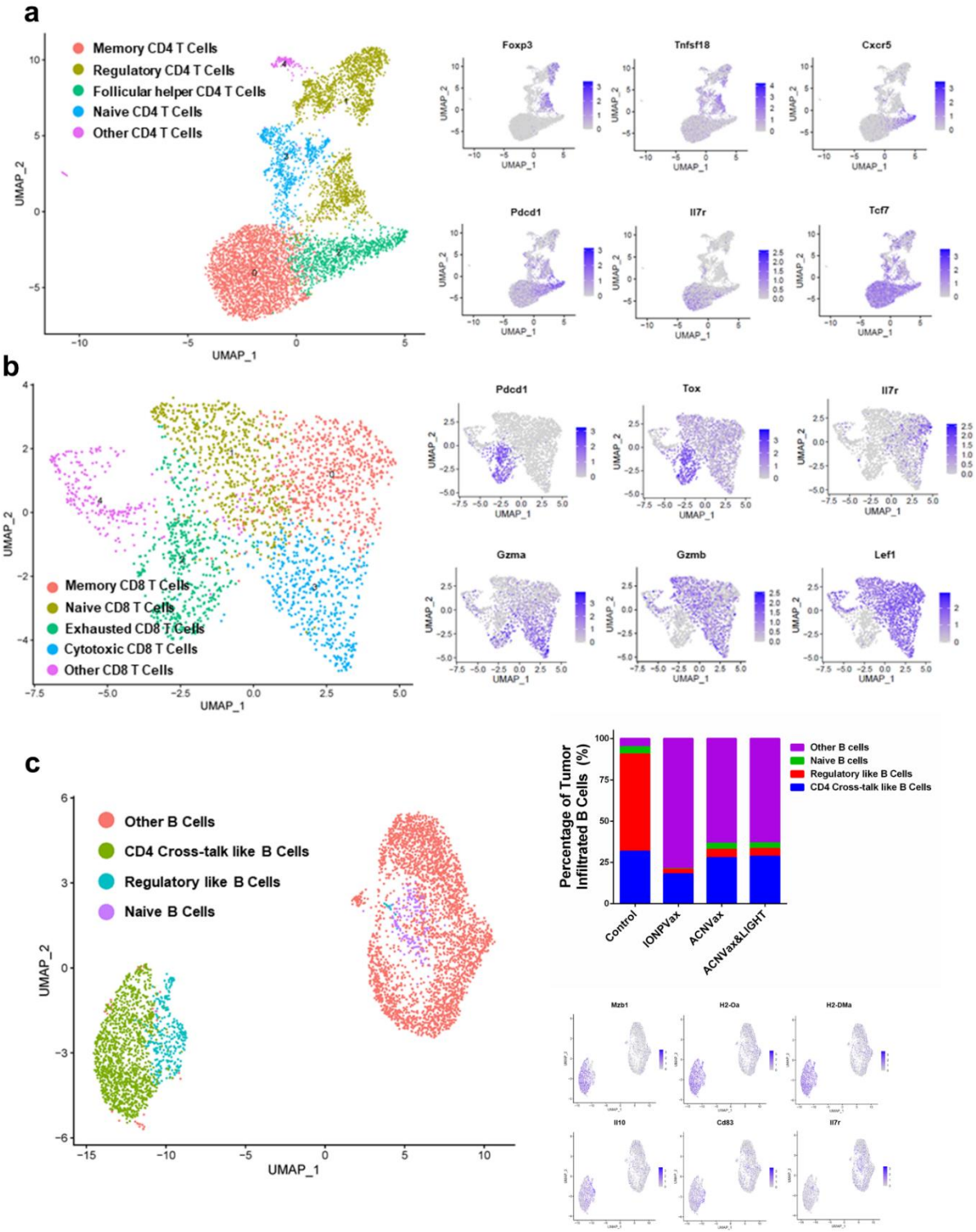

Figure S24. ACNVax induced various gene expression in different sub-populations of CD4 T cells, CD8 T cells, and B cells. Uniform manifold approximation and projection (UMAP) plot and signature genes of tumor infiltrated CD4 T (**a**) and CD8 T (**b**) cells. (**c**) UMAP plot with signature genes and quantification of tumor infiltrated B cell subclusters from single-cell RNA sequencing.

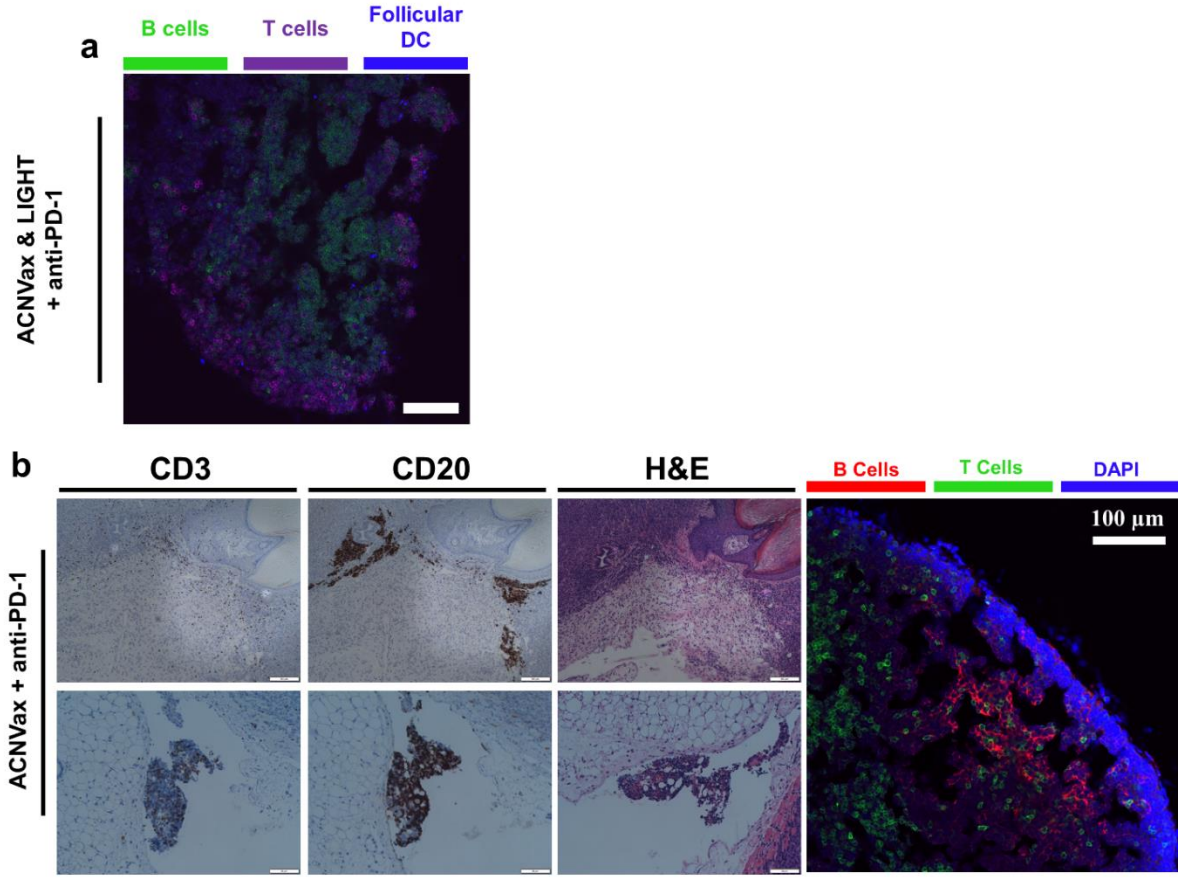

Figure S25. ACNVax increased tertiary lymphoid structure (TLS) formation. (**a**) Confocal imaging and immunohistochemistry staining of tertiary lymphoid structures from mouse tumor samples in the ACNVax&LIGHT plus anti-PD-1 antibody group (14.6 nmol HER2 epitope, 13.9 nmol 2′3′-cGAMP, 50 ng LIGHT, 3 times every 7 days, 100 µg anti-PD-1 antibody biweekly for 3 weeks). Fluorescence immunostaining scale bar is 50 µm, immunohistochemistry staining scale bar is 100 µm. (**b**) Confocal imaging and immunohistochemistry staining of tertiary lymphoid structures from mice tumor from ACNVax plus anti-PD-1 immunized mice. Fluorescent immunostaining scale bar is 100 µm. Tumor tissues were harvested at the endpoint and immediately fixed in paraformaldehyde. For immunohistochemistry staining, antibodies are used to identify different populations of immune cells: B cells (CD20) and T cells (CD3). For fluorescent immunostaining, Alexa Fluor® 594 CD19 (B cells), FITC CD3 (T cells), Alexa Fluor® 647 anti-mouse CD21/CD35 (CR2/CR1) and DAPI Fluoromount-G® were used for confocal imaging. Immunohistochemistry staining scale bar is 100 µm.

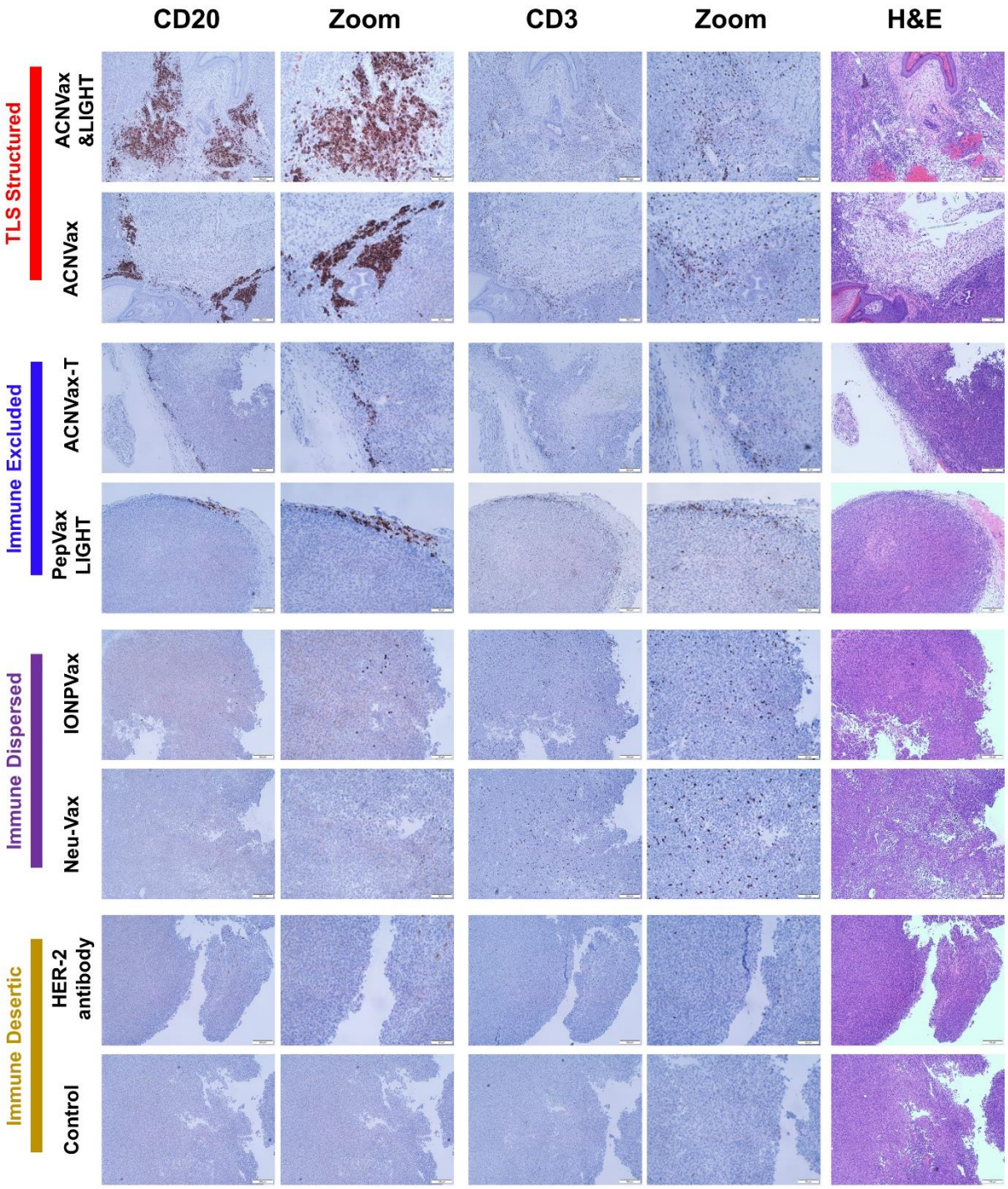

Figure S26. ACNVax induced tertiary lymphoid structure (TLS) formation in comparison with other groups. (**a**) immunohistochemistry staining images of tumor samples different groups. Tumor tissues were harvested at the endpoint and immediately fixed in paraformaldehyde. For immunohistochemistry staining, antibodies are used to identify different populations of immune cells: B cells (CD20) and T cells (CD3). Immunohistochemistry staining scale bar is 100 μm.

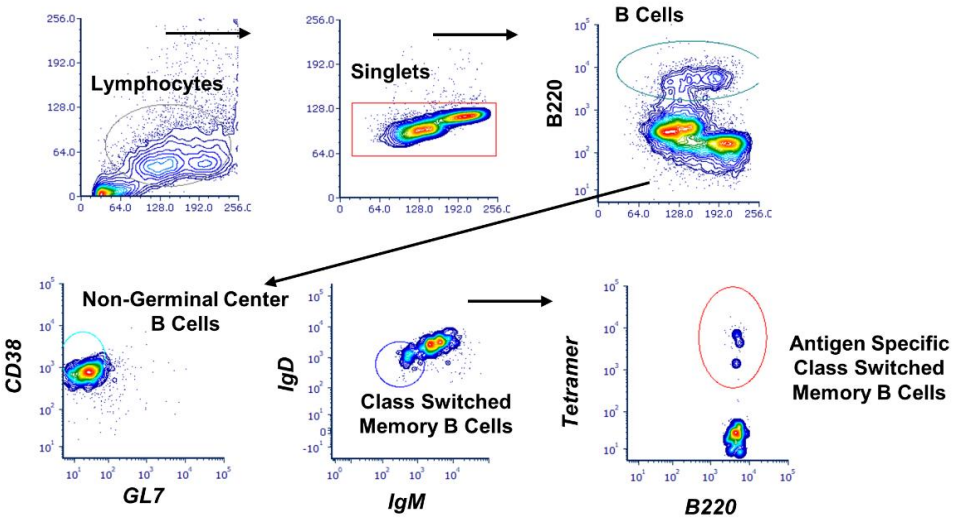

Figure S27. Gating strategy of class switched memory B cells and antigen specific class switched memory B cells from spleen, lymph node, bone marrow and peripheral blood of the mice in Fig. 7a. $B220^{+}$ $CD38^{+}$ $GL\text{-}7^{-}IgD^{-}IgM^{-}$ populations were identified as class switched memory B cells. HER2 tetramer positive class switched memory B cells were identified as antigen specific class switched memory B cells.

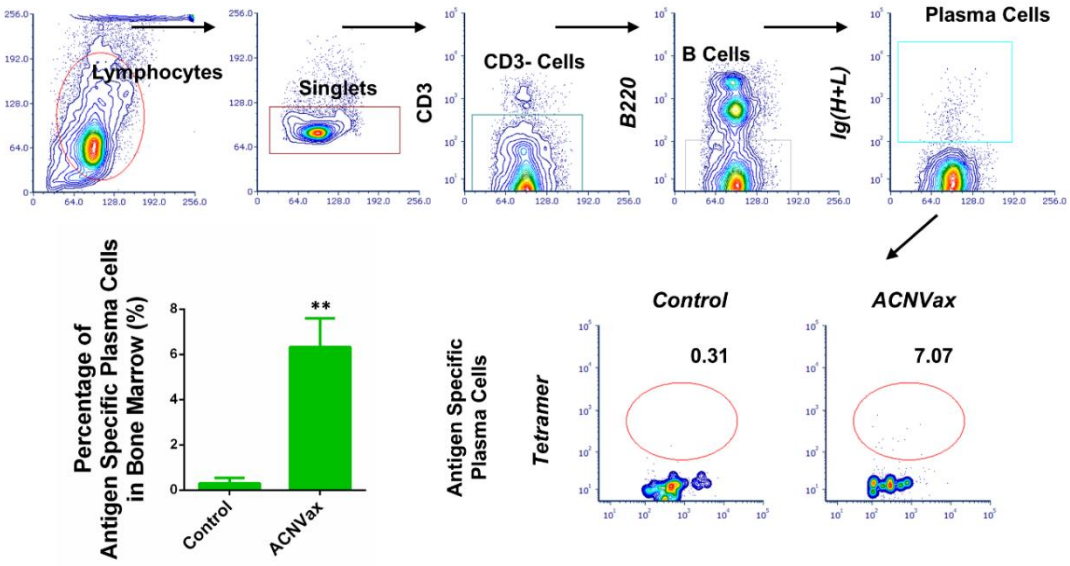

Figure S28. Gating strategy and representative flow cytometry analysis and quantification of antigen specific plasma cells from bone marrow of the mice in Fig. 7a. $CD3^{-}$ $B220^{low}Ig(H+L)^{+}tetramer^{+}$ were identified as antigen specific plasma cells. Data for quantification are shown as mean ± SD, n = 3. Statistical comparisons are based on one-way ANOVA, followed by post hoc Tukey's pairwise comparisons or by Student's unpaired T-test. The asterisks denote statistical significance at the level of * $p < 0.05$, ** $p < 0.01$. ANOVA, analysis of variance; SD, standard deviation.

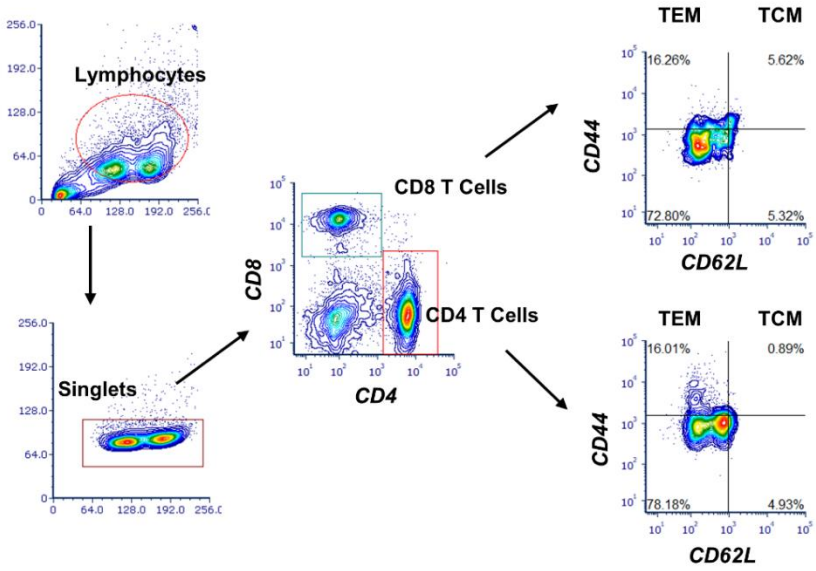

Figure S29. Gating strategy of CD4 T effector memory (TEM), CD4 T central memory (TCM) CD8 TEM and CD8 TCM cells from lymph node and peripheral blood of the mice in Fig. 7a. $CD8^{-}CD4^{+}$ $CD44^{+}$ $CD62L^{-}$ populations were identified as CD4 TEM cells, $CD8^{-}$ $CD4^{+}$ $CD44^{+}$ $CD62L^{+}$ populations were identified as CD4 TCM cells. $CD4^{-}CD8^{+}$ $CD44^{+}$ $CD62L^{-}$ populations were identified as CD8 TEM cells, $CD4^{-}CD8^{+}$ $CD44^{+}$ $CD62L^{+}$ populations were identified as CD8 TCM cells.

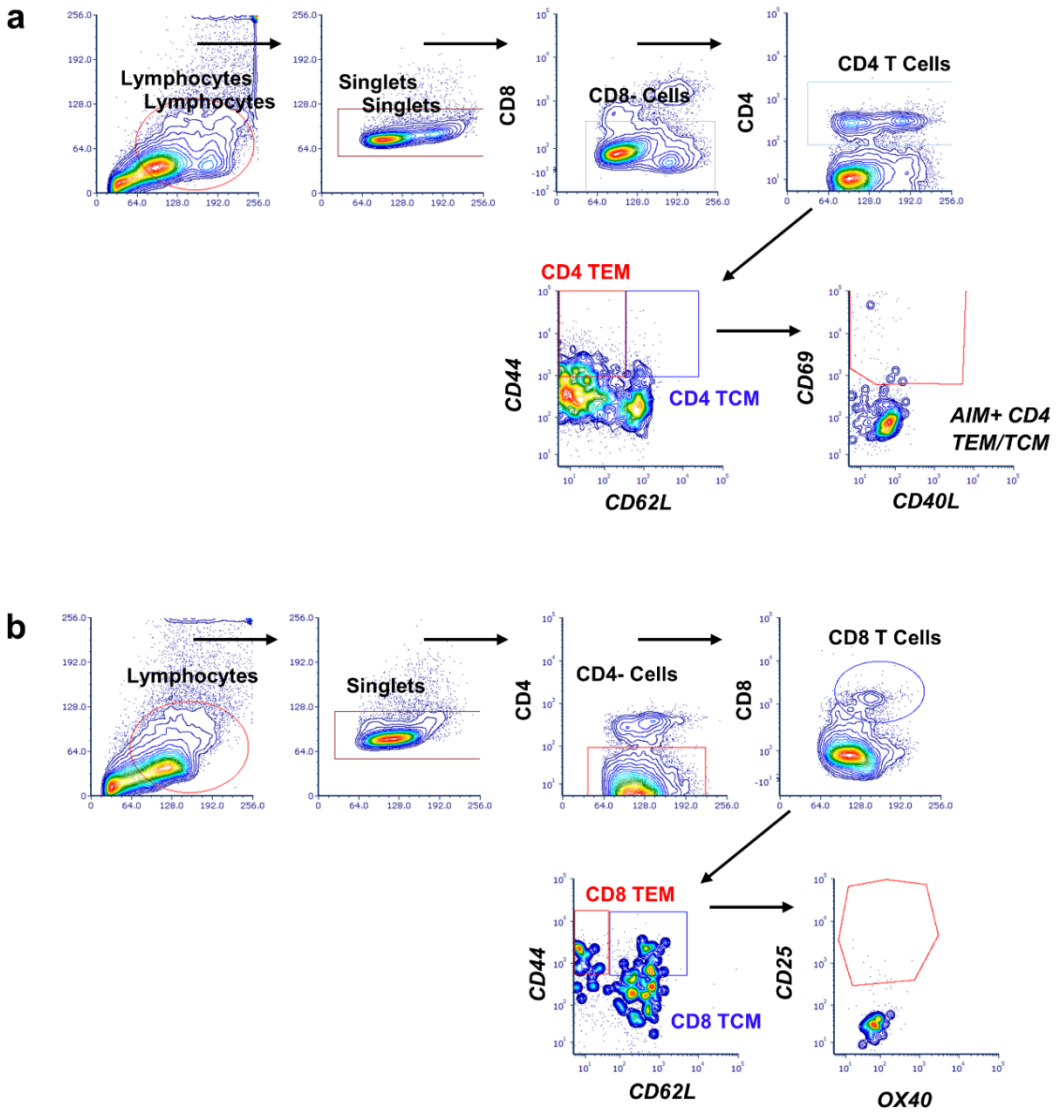

Figure S30. Gating strategy of activation-induced markers assay (AIM) for measuring antigen specific CD4 TEM/TCM cells (a) and CD8 TEM/TCM (b) from spleen of mice in Fig. 7a. $CD8^{-}CD4^{+}$ $CD44^{+}$ $CD62L^{-}$ populations were identified as CD4 TEM cells, $CD8^{-}CD4^{+}$ $CD44^{+}$ $CD62L^{+}$ populations were identified as CD4 TCM cells. $CD69^{+}CD40L^{+/-}$ populations from CD4 TEM/TCM cells were identified as AIM^{+} CD4 TEM/TCM cells. $CD4^{-}CD8^{+}$ $CD44^{+}$ $CD62L^{-}$ populations were identified as CD8 TEM cells, $CD4^{-}CD8^{+}$ $CD44^{+}$ $CD62L^{+}$ populations were identified as CD8 TCM cells. $CD25^{+}OX40^{+/-}$ populations from CD8 TEM/TCM cells were identified as AIM^{+} CD8 TEM/TCM cells.

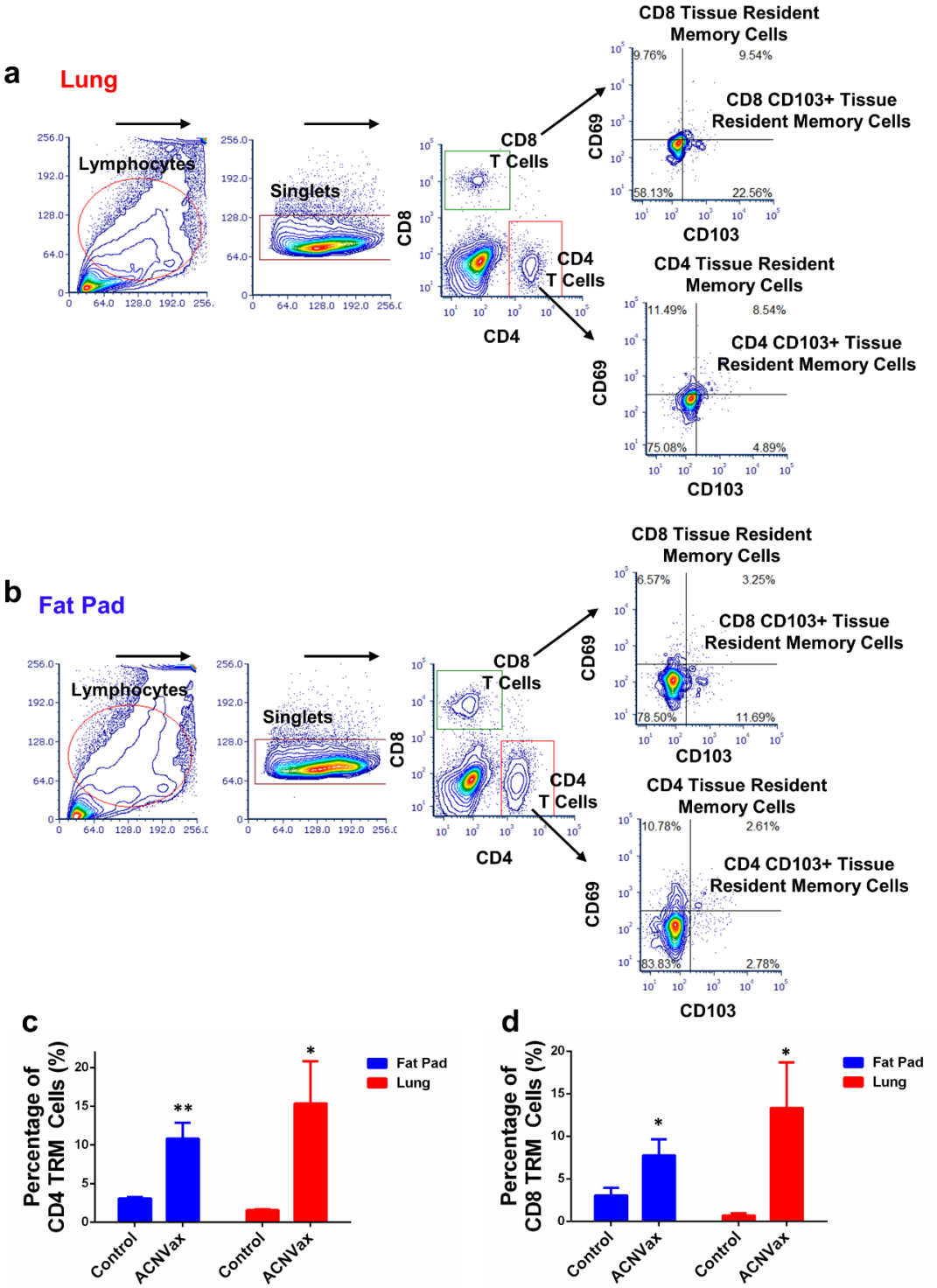

Figure S31. Gating strategy of flow cytometry analysis of CD4 Tissue resident memory T (TRM, c) and CD8 TRM (d) cells from Lung (a) and Fat pad (b). Representative flow cytometry analysis and quantification of CD4 Tissue resident memory T (TRM, **c**) and CD8 TRM (**d**) cells from Lung (**a**) and Fat pad (**b**) of the mice in **Fig. 6a**. $CD8^{-}CD4^{+}$ $CD69^{+}$ $CD103^{-/+}$ populations were identified as CD4 TRM cells. $CD4^{-}CD8^{+}$ $CD69^{+}$ $CD103^{-/+}$ populations were identified as CD8 TRM cells. Data for quantification are shown as mean ± SD, n = 3. Statistical comparisons are based on one-way ANOVA, followed by post hoc Tukey's pairwise comparisons or by Student's unpaired T-test. The asterisks denote statistical significance at the level of * $p < 0.05$, ** $p < 0.01$. ANOVA, analysis of variance; SD, standard deviation.

Mathematical Modeling:

Gold Nanoparticle (AuNP) Loading per Viral antigen cluster mimicry nanovaccine (ACN)

The extent of gold nanoparticle (AuNP) loading to Viral antigen cluster mimicry nanovaccine (ACN) surfaces was determined by ICP-MS determination of total elemental gold (Au) and iron (Fe) weights. These weights were then utilized to quantify total number spheres of a given element and particle size based on previously reported methods[3, 4]. The ratio of these experimental values was then interpreted as AuNPs per ACN, or the number of AuNPs per single IONP core.

Due to the crystalline structure of iron-oxide nanoparticles, it is possible to quantify the number of nanoparticles per unit Fe based on known particle size accordingly to previously establish methodologies (**Table S1**)[3]. Using transmission electron microscopy (TEM), the exact particle size of iron-oxide nanoparticles was quantified using the ImageJ software. The particle size of the polymer-coated iron-oxide nanoparticle core of the ACN was 15 nm, while the particle size of the lipid-coated iron-oxide nanoparticle control was 30 nm. Based on the known unit cell volume of iron-oxide (Fe_3O_4) and quantified particle size, the number of nanoparticles per gram Fe was determined to be $1.5x10^{17}$ and $1.9x10^{16}$ for 15 nm and 30 nm cores, respectively (**Table S1**).

The number of gold nanoparticles per unit Au was quantified by two considerations. First, based on literature values reported[4], AuNPs with 3 nm diameters have 479 gold atoms per nanoparticle, which is 56% of the number of gold atoms per solid gold metallic colloids of the same diameter (835 gold atoms per nanoparticle). Therefore, by conversion from weight of Au to atoms of Au through Avogadro's Number it is possible to quantify the number of gold nanoparticle per unit Au. Quantification by this methodology revealed that number gold nanoparticle per gram Au was $6.38x10^{18}$ (**Table S2**). Second, based on literature values reported for the mass of a single AuNP for 2 nm, 5 nm and 10 nm particle size, the mass of a single 2 nm AuNP was interpolated based on curve fitting. Through curve fitting, the mass of a single 3 nm AuNP was determined to be $2.67x10^{19}$ grams or $3.67x10^{18}$ AuNPs per gram Au (**Table S2**). Notably, this quantified value matches those values reported for solid gold colloids based on 835 gold atoms per nanoparticle and therefore was not considered truly representative of our materials.

Table S1. Iron-oxide nanoparticle calculations. Quantification of total number of spheres per unit Fe and total surface area per unit Fe for 15-nm and 30-nm iron-oxide nanocrystal cores. Calculations were performed based on equations outlined previously[3].

Description	Value
Unit cell volume of Fe_3O_4	0.5905 nm^3
Fe atoms per unit Fe_3O_4 cell	24
Molecular weight of Fe	55.85 g/mole
Avogadro's Number	6.022×10^{23}
Volume of 15 nm IONP core – single sphere	1766 nm^3
Volume of 30 nm IONP core – single sphere	14130 nm^3
Surface Area per Sphere - 15 nm IONP core	707 nm^2
Surface Area per Sphere - 30 nm IONP core	2826 nm^2
Number of Fe atoms per g Fe	1.08×10^{22}
Number of Fe_3O_4 unit cells per g Fe	4.5×10^{20}
Number of Fe_3O_4 unit cells per Single Sphere – 15 nm IONP core	2944
Number of Fe_3O_4 unit cells per Single Sphere – 30 nm IONP core	23550
Total Number of Spheres per g Fe – 15 nm IONP core	1.5×10^{17}
Total Number of Spheres per g Fe – 30 nm IONP core	1.9×10^{16}
Total Surface Area per g Fe – 15 nm IONP core	1.1×10^{20} nm^2
Total Surface Area per g Fe – 30 nm IONP core	2.7×10^{20} nm^2

Table S2. Gold nanoparticle calculations. Quantification of total number of spheres per unit Au for 3 nm AuNPs

Description	Value
Method 1	
Density of Gold	19.32 g/cm^3
Atomic Number	197
Average # of Gold Atoms per AuNP (3 nm)	479
Number of AuNPs per g Fe (3 nm)	6.38E+18
Method 2	
Mass of Single AuNP (g)	2.67E-19
Number of AuNPs per g Au (3 nm)	3.67E+18

Gold Nanoparticle Spatial Distribution –Inter-Nanoparticle Distance

The distance between AuNPs on ACN surfaces was modeled based on two methodologies. The first technique was based on the arc length equation for a circle. If homogeneous distribution of AuNPs on a sphere is assumed, the loading of 2, 6 and 14 AuNPs on ACN surface will yield AuNPs in a single plane (circle) oriented at central angles equivalent to 180º, 90º and 45º, respectively. Using the arc length equation for a circle with radius 7.5 nm, 2, 6 and 14 AuNPs will be located 23.6, 11.8 and 5.9 nm apart, respectively. Plotting these three points and using a power function curve fitting model ($R^2 = 0.99$) allows for interpolations of inter-nanoparticle distances between 2-14 AuNPs per ACN surface (**Fig. S1c-1e**, **Table S3**). The benefit of this technique is that it accounts for arc length and is not a straight-line distance calculation. However, this model represent AuNPs are single points and only has three points for the curve fitting model thereby limiting potential power and accuracy.

The second technique used to quantify inter-nanoparticle distance on ACN surfaces was based on a triangulation methodology. With the number of AuNPs per ACN surface known and assuming homogeneous distribution of AuNPs on a sphere around a single central focal point, AuNPs can be triangulated. For AuNP per ACN equal to or greater than 4, the number of triangles formed around a central focal point is 2n, where n is the number of AuNPs per ACN.

$$AuNP\ Triangles\ per\ IONP\ core\ = AuNP\ per\ IONP\ core \times 2$$

With the number of triangles determined, the surface occupied by a single triangle was quantified given the surface area of spherical ACN with 7.5 nm radius.

$$Surface\ Area\ per\ Triangle = \frac{Surface\ Area\ of\ IVLN}{Number\ of\ Triangles}$$

Assuming an equilateral triangle, the surface area of a single triangle can be used to determine the length of a side of the triangle, and therefore the distance between AuNPs represented as single points. By subtracting 2x the radius of the AuNPs, a better surface to surface contact distance can be interpreted (**Fig. S1c-1e**, **Table S4**).

$$Distance\ between\ AuNPs = \sqrt{\frac{4\ \times Triangle\ Surface\ Area}{\sqrt{3}}} - (\ 2 \times AuNP\ radius)$$

The benefit of this technique is that does not rely on interpolation. However, this model is limited due to the reliance of straight-line distances between AuNPs.

Table S3. Inter-nanoparticle distance: Arc Length Interpolation Model. Interpolation data set for inter-AuNP distances based on AuNP per ACN determined by ICP-MS (**Fig. 1c**) and the curve fitting model presented in **Fig. S1c-1e** ($y = 39.51x^{-.708}$, $R^2 = 0.99$).

Au/Fe Ratio (wt/wt)	AuNP per ACN	Inter-Nanoparticle Distance Arc Length (nm)
0.05	2.1	23.18
0.1	4.2	14.19
0.15	6.4	10.65
0.2	8.5	8.69
0.25	10.6	7.42
0.3	12.7	6.52
0.35	14.9	5.84
0.4	17.0	5.32

Table S4. Inter-nanoparticle distance: Triangulation Model. Data set for inter-AuNP distances based on AuNP per ACN determined by ICP-MS (**Fig. 1c**) and mathematic modeling presented above, and curve fitting model presented in **Fig. S1c-1e** ($y = 28.69x^{-.649}$, $R^2 = 0.99$).

Au/Fe Ratio (wt/wt)	AuNP per ACN	Inter-Nanoparticle Distance Arc Length (nm)
0.05	2.1	17.10
0.1	4.2	11.36
0.15	6.4	8.82
0.2	8.5	7.30
0.25	10.6	6.27
0.3	12.7	5.50
0.35	14.9	4.91
0.4	17.0	4.43

Table S5. ACN material properties before and after peptide conjugation under saturating conditions.

	ACN	ACNVax
Particle Size (nm)	**38 ± 3**	**44 ± 2**
Polydispersity Index (PDI)	**0.112 ± 0.04**	**0.087 ± 0.03**
Zeta-Potential (mV)	**-16 ± 4**	**-17 ± 1**

Table S6. Lipid-coated IONP material properties before and after peptide conjugation under saturating conditions.

	Lipid IONP	**IONPVax**
Particle Size (nm)	**38 ± 4**	**48 ± 5**
Polydispersity Index (PDI)	**0.068 ± 0.05**	**0.074 ± 0.02**

Table S7. Heavy metal labeled antibody panel for CyTOF analysis in Lymph node (**Fig. 3b**).

Channel	**Specificity**	**Clone**	**Vendor**
112Cd	CD19	6D5	Life Technologies
141Pr	IFNg	XMG1.2	Biolegend
142Nd	CD86	GL-1	Biolegend
143Nd	CD80	16-10A1	Biolegend
144Nd	IgM	RMM-1	Biolegend
145Nd	CD4	RM4-5	Biolegend
146Nd	CD45R (B220)	RA3-6B2	Biolegend
147Sm	CD206	C068C2	Biolegend
148Nd	CD138	281-2	Biolegend
149Sm	CD8	53-6.7	Biolegend
150Nd	mPDCA-1 (CD317)	129C1	Biolegend
151Eu	CD49b (DX5)	DX5	Biolegend
152Sm	Ly-6C	HK1.4	Novus Biologicals
153Eu	IFNb	7F-D3	Abcam
154Sm	CD11c	N418	Biolegend
155Gd	IA-IE	M5/114.15.2	Biolegend
156Gd	CD25	3C7	Biolegend
158Gd	IgD	11-26c-2a	Biolegend
159Tb	Ly-6G	1A8	Biolegend
160Gd	Il-4	11B11	Biolegend
161Dy	Il-17a	TC11-18H10.1	Biolegend
162Dy	TCRγδ	GL3	Biolegend
163Dy	CD64	X54-5/7.1	Biolegend
164Dy	Il-10	JES5-16E3	Biolegend
165Ho	CD115	AFS98	Biolegend
166Er	CXCR5	614641	Novus Biologicals
167Er	FR4	TH6	Biolegend
168Er	CD24	M1/69	Biolegend
169Tm	CXCR4	L276F12	Biolegend
170Er	CD62L	MEL-14	Biolegend
171Yb	CD44	IM7	Biolegend

172Yb	CD11b	M1/70	Fluidigm
173Yb	PD-1	RMP1-30	Biolegend
174Yb	GL7	GL7	Biolegend
175Lu	F4/80	BM8	Biolegend
176Yb	GmzB	GB11	Abcam
209Bi	CD3	145-2C11	Biolegend
89Y	mCD45	30-F11	Fluidigm
195Pt	Cisplatin	Live/Dead	Fluidigm
191/193Ir	DNA Intercalator	DNA	Fluidigm

Table S8. Murine HER-2 antibody (Murine 2C4) Amino Acids Sequences.

Heavy Chain Variable Region	EVQLQQSGPELVKPGTSVKISCKASGFTFTDYTMDWVKQSHGK SLEWIGDVNPNSGGSIYNQRFKGKASLTVDRSSRIVYMELRSLT FEDTAVYYCARNLGPSFYFDYWGQGTTLTVSS
Heavy Chain Constant Region (Mouse IgG2a)	AKTTAPSVYPLAPVCGDTTGSSVTLGCLVKGYFPEPVTLTWNS GSLSSGVHTFPAVLQSDLYTLSSVTVTSSTWPSQSITCNVAHPA SSTKVDKKIEPRGPTIKPCPPCKCPAPNLLGGPSVFIFPPKIKDVL MISLSPIVTCVVVDVSEDDPDVQISWFVNNVEVHTAQTQTHRE DYNSTLRVVSALPIQHQDWMSGKEFKCKVNNKDLPAPIERTIS KPKGSVRAPQVYVLPPPEEEMTKKQVTLTCMVTDFMPEDIYVE WTNNGKTELNYKNTEPVLDSDGSYFMYSKLRVEKKNWVERN SYSCSVVHEGLHNHHTTKSFSRTPGK
Light Chain Variable Region	DTVMTQSHKIMSTSVGDRVSITCKASQDVSIGVAWYQQRPGQS PKLLIYSASYRYTGVPDRFTGSGSGTDFTFTISSVQAEDLAVYY CQQYYIYPYTFGGGTKLEIK
Light Chain Constant Region (Mouse Ig Kappa)	RADAAPTVSIFPPSSEQLTSGGASVVCFLNNFYPKDINVKWKID GSERQNGVLNSWTDQDSKDSTYSMSSTLTLTKDEYERHNSYTC EATHKTSTSPIVKSFNRNEC

Table S9. Heavy metal labeled antibody panel for CyTOF analysis in Tumor (**Fig. 5a**).

Channel	**Specificity**	**Clone**	**Vendor**
112Cd	CD19	6D5	Life Technologies
141Pr	IFNg	XMG1.2	Biolegend
142Nd	CD86	GL-1	Biolegend
143Nd	CD80	16-10A1	Biolegend
144Nd	Siglec-F	E50-2440	BD Biosciencies
145Nd	CD4	RM4-5	Biolegend
146Nd	CD45R (B220)	RA3-6B2	Biolegend
147Sm	CD206	C068C2	Biolegend
148Nd	CD138	281-2	Biolegend
149Sm	CD8	53-6.7	Biolegend
150Nd	mPDCA-1 (CD317)	129C1	Biolegend
151Eu	CD49b (DX5)	DX5	Biolegend
152Sm	Ly-6C	HK1.4	Novus Biologicals

154Sm	CD11c	N418	Biolegend
155Gd	IA-IE	M5/114.15.2	Biolegend
156Gd	CD25	3C7	Biolegend
158Gd	TIM-3	RMT3-23	Biolegend
159Tb	Ly-6G	1A8	Biolegend
160Gd	Il-4	11B11	Biolegend
161Dy	Il-17a	TC11-18H10.1	Biolegend
162Dy	TCRγδ	GL3	Biolegend
163Dy	Il-17f	316016	Novus Biologicals
164Dy	Il-10	JES5-16E3	Biolegend
165Ho	CD115	AFS98	Biolegend
166Er	CXCR5	614641	Novus Biologicals
167Er	FR4	TH6	Biolegend
168Er	NOS2	5C1B52	Biolegend
169Tm	Ly-6A/E (Sca-1)	D7	Biolegend
170Er	CD62L	MEL-14	Biolegend
171Yb	CD44	IM7	Biolegend
172Yb	CD11b	M1/70	Fluidigm
173Yb	PD-1	RMP1-30	Biolegend
174Yb	CTLA-4	UC10-4B9	Biolegend
175Lu	F4/80	BM8	Biolegend
176Yb	GmzB	GB11	Abcam
209Bi	CD3	145-2C11	Biolegend
89Y	mCD45	30-F11	Fluidigm
195Pt	Cisplatin	Live/Dead	Fluidigm
191/193Ir	DNA Intercalator	DNA	Fluidigm

Supporting Methods

Preparation and characterization of different nanovaccine controls.

AuNPVax

The synthesis of AuNP is the same as that in the preparation of ACN. AuNPs (2 nm) were synthesized by reacting sodium sulfide (Na2S) as the reducing reagent with gold in the form of chloroauric acid (HAuCl4). HER2 peptide was added to AuNPs following the same amount in the preparation of ACN in Milli-Q water and incubated overnight at 4 °C, and purified by magnetic separation overnight at 4 °C. AuNP-B/CD4 were imaged by STEM using a JEOL 2100F with a CEOS probe corrector.

LipoVax

Liposome were prepared following the thin-film method[5]. DSPC (Avanti. Birmingham, Al), Cholesterol (Sigma-Aldrich, St. Louis, MO) and PEG2000-DSPE-MAL (Avanti. Birmingham,

Al) were dissolved in chloroform at the weight ratio of 20:1:5 and dried under reduced pressure at 37 ºC until they formed a thin lipid film. The lipid film was hydrated with warm PBS, followed by sonication with a bath type sonicator. HER2 peptides were conjugated to PEG2000-DSPE-MAL on the surface of liposome via maleimide-thiol chemistry. HER2 peptide was added to liposome at a 5× weight ratio excess in Milli-Q water and incubated overnight at 4 °C, and purified either by magnetic separation overnight at 4 °C. The hydrodynamic particle size, polydispersity index and zeta potential were evaluated with a Malvern Zetasizer Nano-ZS in Milli-Q water at 25 °C.

Confocal imaging for B Cell uptake *in-vitro*

ACNVax-EDFITC, IONPVax-EDFITC and PepVax-EDFITC peptide cellular uptakes were evaluated in primary B-cells isolated from murine spleens using an EasySep Mouse B-cell isolation kit. Cells were incubated with ACNVax-EDFITC, IONPVax-EDFITC and PepVax-EDFITC (25 µg/mL HER2-B/CD4 epitope) for 15 mins, 30 mins and 60 mins. Cells were then washed, fixed and plated onto eight-well glass chambers pretreated with 0.1% poly-l-lysine (LabTech II) on ice for at least 4 hours before confocal imaging.

***In-vitro* B cell uptake**

ACNVax and IONPVax cellular uptakes were evaluated in primary B-cells isolated from murine spleens using an EasySep Mouse B-cell isolation kit. Nanoparticle samples were incubated at 50 µg/mL Fe with cells for 18 hours in blank RPMI media at 37 °C, 5% CO_2/95% air atmosphere and approximately 85% relative humidity. After 18 hours, cells were lifted by cell scraping and washed thrice with PBS. Following the wash steps, resulting cell pellets were re-suspended in 1 mL of PBS, cell counted and then digested in 1 mL aqua regia (1:3 molar ratio nitric acid: hydrochloric acid) for analysis by ICP-MS.

Quantification of nanoparticle delivery to lymph nodes *in-vivo*

Mice were injected subcutaneously in the left hock with either IONP or ACN at a dose of 200 µg Fe per mouse. At the designated time intervals, mice were sacrificed and lymph nodes of interest were dissected for *ex-vivo* analysis. The extent of nanoparticle delivery to the lymph nodes was quantified using ICP-MS based on previously reported protocols[6].

Quantification of peptide delivery to lymph nodes *in-vivo*

To facilitate quantification of peptide delivery to lymph nodes, lysine terminally modified HER2 peptides were chemically conjugated to sulfo-Cy5.5 NHS Ester. This conjugation was carried out at a 5-fold molar excess of sulfo-Cy5.5 NHS Ester to PepVax. IONPVax-Cy5.5 and

ACNVax-Cy5.5 were subjected to Cy5.5 functionalization after initial peptide conjugation was completed to enable facile purification of excess fluorescent dye by magnetic separation. Subsequent to Cy5.5 functionalization, mice were injected as previously stated. After 3 hours, mice were sacrificed and lymph nodes of interest were dissected for *ex-vivo* analysis by IVIS imaging. IVIS imaging was utilized for semi-quantification of peptide delivery in terms of radiant efficiency.

3D imaging of in vivo lymph node distribution

To determine the ACNVax (conjugated to ED-FITC labeled HER2-B/CD4 peptide, 233.6 nmol HER2 epitope) distribution, lymph nodes were harvested 12 hours after subcutaneous dosing. Harvested tissues were immediately processed following iDisco protocol for clearing and staining of antibodies. Brilliant Violet 421 B220, Alexa Fluor® 594 CD 3 and Alexa Fluor® 647 CD169 were validated and used for lymph node immune fluorescence staining. 3D imaging was then conducted on Bruker MuVi SPIM.

Sample Pretreatment with Methanol

1. Dehydrate with methanol/H2O series: 20%, 40%, 60%, 80%, 100%; 1h each.
2. Wash further with 100% methanol for 1h and then chill the sample at 4°c.
3. Overnight incubation, with shaking, in 66% DCM / 33% Methanol at RT
4. Wash twice in 100% Methanol at RT, and then chill the sample at 4°c
5. Bleach in chilled fresh 5%H2O2 in methanol (1 volume 30% H2O2 to 5 volumes MeOH), overnight at 4°c.
6. Rehydrate with methanol/H2O series: 80%, 60%, 40%, 20%, PBS; 1h each at RT.
7. Wash in PTx.2 RT 1h x2 at RT.

Immunolabeling

1. Incubate samples in Permeabilization Solution, 37°C **n**/2 days (max. 2 days)
2. Block in Blocking Solution, 37 °, **n**/2 days (max. 2 days).
3. Incubate with primary antibody in PTwH/5%DMSO/3% Donkey Serum, 37°, n days.
4. Wash in PTwH for 4-5 times until the next day.

Clearing

1. Dehydrate in methanol/H2O series: 20%, 40%, 60%, 80%, 100%, 100%; 1hr each at RT. Can be left optionally overnight at RT at this point.
2. 3H incubation, with shaking, in 66% DCM / 33% Methanol at RT
3. Incubate in 100% DCM (Sigma 270997-12X100ML) 15 minutes twice (with shaking) to wash the MeOH.

4. Incubate in Dibenzyl Ether (DBE, Sigma 108014-1KG) (no shaking). The tube should be filled almost completely with DBE to prevent the air from oxidizing the sample. Before imaging, invert the tube a couple of time to finish mixing the solution

References

(1) Mingueneau, M.; Krishnaswamy, S.; Spitzer, M. H.; Bendall, S. C.; Stone, E. L.; Hedrick, S. M.; Pe'er, D.; Mathis, D.; Nolan, G. P.; Benoist, C. Single-cell mass cytometry of TCR signaling: amplification of small initial differences results in low ERK activation in NOD mice. *PNAS* **2014**, *111* (46), 16466-16471. DOI: 10.1073/pnas.1419337111.
(2) Billi, A. C.; Gharaee-Kermani, M.; Fullmer, J.; Tsoi, L. C.; Hill, B. D.; Gruszka, D.; Ludwig, J.; Xing, X.; Estadt, S.; Wolf, S. J.; et al. The female-biased factor VGLL3 drives cutaneous and systemic autoimmunity. *JCI Insight* **2019**, *4* (8). DOI: 10.1172/jci.insight.127291.
(3) Kokate, M.; Garadkar, K.; Gole, A. One pot synthesis of magnetite–silica nanocomposites: applications as tags, entrapment matrix and in water purification. *J Mater Chem A* **2013**, *1* (6), 2022-2029, 10.1039/C2TA00951J. DOI: 10.1039/C2TA00951J.
(4) Lu, Y.; Wang, L.; Chen, D.; Wang, G. Determination of the concentration and the average number of gold atoms in a gold nanoparticle by osmotic pressure. *Langmuir* **2012**, *28* (25), 9282-9287. DOI: 10.1021/la300893e.
(5) Wang, N.; Chen, M.; Wang, T. Liposomes used as a vaccine adjuvant-delivery system: From basics to clinical immunization. *J control release* **2019**, *303*, 130-150. DOI: 10.1016/j.jconrel.2019.04.025.
(6) Chertok, B.; Cole, A. J.; David, A. E.; Yang, V. C. Comparison of electron spin resonance spectroscopy and inductively-coupled plasma optical emission spectroscopy for biodistribution analysis of iron-oxide nanoparticles. *Mol pharmaceutics* **2010**, *7* (2), 375-385. DOI: 10.1021/mp900161h.